2008

Investigation of laser peening effects on hydrogen charged stainless steels

Tania M. Zaleski
San Jose State University

INVESTIGATION OF LASER PEENING EFFECTS ON HYDROGEN CHARGED STAINLESS STEELS

A Thesis

Presented to

The Faculty of the Department of Physics

San José State University

In Partial Fulfillment

of the Requirements for the Degree

Master of Science

by

Tania M. Zaleski

December 2008

This work was performed under the auspices of the U.S. Department of Energy by Lawrence Livermore National Laboratory in part under Contract W-7405-Eng-48 and in part under Contract DE-AC52-07NA27344.

SAN JOSE STATE UNIVERSITY
The Undersigned Thesis Committee Approves the Thesis Titled

INVESTIGATION of LASER-PEENING EFFECTS on HYDROGEN CHARGED STAINLESS STEELS

by
Tania Zaleski

APPROVED FOR THE DEPARTMENT OF PHYSICS

Prof. Ken Wharton, PhD Department of Physics	11/10/08 Date
Prof. Peter Beyersdorf, PhD Department of Physics	11/10/08 Date
Nancy Yang Sandia National Laboratory	11/5/08 Date
Chris San Marchi, PhD Sandia National Laboratory	11/5/08 Date

APPROVED FOR THE UNIVERSITY

Associate Dean	12/17/08 Date

ABSTRACT

INVESTIGATION ON LASER-PEENING EFFECTS ON HYDROGEN CHARGED STAINLESS STEELS

by Tania M. Zaleski

Hydrogen-rich environments such as fuel cell reactors can exhibit damage caused by hydrogen permeation in the form of corrosion cracking by lowering tensile strength and decreasing material ductility.

Coatings and liners have been investigated, but there were few shot-peening or laser peening studies referenced in the literature with respect to preventing hydrogen embrittlement. The surface compressive residual stress induced by laser peening had shown success in preventing stress corrosion cracking (SCC) for stainless steels in power plants [1,2]. The question arose if the residual stresses induced by laser peening could delay the effects of hydrogen in a material.

This study investigated the effect of laser peening on hydrogen penetration into metal alloys. Three areas were studied: laser peening, hydrogenation, and hydrogen detection. This study demonstrated that laser peening does not reduce the hydrogen permeation into a stainless steel surface nor does it prevent hydrogen embrittlement. The effect of laser peening to reduce hydrogen-assisted fatigue was unclear.

ACKNOWLEDGEMENTS

The author would like to thank Nancy Yang for mentoring and Chris San Marchi for his hydrogen expertise. Both Nancy and Chris are at Sandia National Laboratory, where much of the sample preparation and testing took place. Lloyd Hackel's support and guidance, while initially leading the laser peening project at LLNL and now at Metal Improvement Company, has been invaluable. The author greatly appreciates the funding for much of this research as provided by the NIF/PS&A program from Dr. Ed Moses and Dr. Chris Barty. The author would also like to thank Rich Shuttlesworth from LLNL and Jack Rybak previously at LLNL, now at MIC; who spent many hours machining and processing the coupons in this study. The time spent with the people from the MC^2 Facility at SJSU (through the Defense Microelectronics Activity Cooperative Agreement #H94003-08-0806) is greatly appreciated. Thanks to Professor Mike Hill and Jon Rankin for many useful discussions on testing fatigue life and crack growth.

Patrick, thank you for pushing me to write.

TABLE OF CONTENTS

LIST OF FIGURES

LIST OF TABLES

1. INTRODUCTION

1.1. Hydrogen Storage Issues

Moving toward a hydrogen economy will require production, storage and transportation of large quantities of hydrogen under various operating conditions. Currently, there are a number of technical problems that threaten the long-term usage of low cost steels for storage and transportation of hydrogen. Molecular hydrogen can dissociate at metal surfaces and diffuse into the bulk, greatly reducing ductility and ability to withstand cyclic loads. Hydrogen embrittlement of reactor vessels, transport pipelines, and storage containers, together with potential explosive scenarios for hydrogen accumulation in enclosed spaces, is a major safety and environmental concern for hydrogen fuel users. In addition, atomic power plants could greatly benefit from improved lifetime of components exposed to hydrogen, deuterium, and tritium [3]. This project investigates the physical and mechanical benefits of applied compressive stresses to the mitigation of hydrogen-induced effects in metals and alloys. Predicting and solving problems related to hydrogen embrittlement will have a tremendous impact on materials exposed to radiation and a future hydrogen economy.

Hydrogen-induced embrittlement (or degradation) in metals occurs in a number of forms but the common features are residual or applied tensile stress and the presence of atomic hydrogen or hydride compounds in the material structure [4]. A specific example is the cracking of weldments when exposed to

conditions that allow hydrogen to diffuse into the component [5]. This phenomenon is not completely understood and the detection of hydrogen-induced damage (before sudden catastrophic failure) remains a major technical challenge. Issues of importance to hydrogen users include:

Permeation: hydrogen has high permeation rates through low alloy pressure vessel and pipeline steels (as much as 10^5 greater than stainless steels).

Hydrogen-assisted fracture: dissolved hydrogen assists nucleation and propagation of cracks in steels by enhancing plasticity and affecting the strength of interfaces such as grain boundaries.

Hydrogen attack: in some systems under specific environmental conditions (such as high temperature), dissolved hydrogen can irreversibly react with the microstructure to produce brittle phases or in situ cracks.

1.2. Hydrogen Damage Formation

When the hydrogen atoms permeate into the metal the travel through the crystal lattice along microstructural channels or through innerstitial lattice sites [5, 6, 7]. The majority of these sites are ordinary sites described by the normal enthalpy of solution with respect to the atmosphere of hydrogen where the lattice is in contact [4]. However, a fraction of the sites can be described as extraordinary sites which are energetically favorable for the occupancy of hydrogen such that the transition of the hydrogen from an ordinary to extraordinary site coincides with a negative change in energy [4]. At these

locations the hydrogen collects because the energetic potential is favored.

Symons summarizes previous work on the mechanism for hydrogen embrittlement in materials by describing three theories [7]. The first mechanism originally proposed by Steigerwald and furthered by Oriani and Josephic details a decohesion mechanism where hydrogen collects in microvoids which coalesce, decreasing the cohesive energy between atoms and promoting cleavage [8,9]. A second theory proposed by Beachem describes how hydrogen alters deformation behavior by increasing the mobility of dislocations [10, 11, 12]. This theory is furthered by Lee and Costa where hydrogen alters deformation by collecting along slip planes [13,14]. A third mechanism proposed by Zapfe and Sims describes hydrogen accumulating at grain boundaries, causing local pressure and reducing the stress required to initiate or increase void coalescence [15].

1.3. Industry Mitigation Techniques

The conventional methods used by industry to mitigate hydrogen-induced damage in metals include reduction of hydrogen charging, reduction of tensile stress in components, and the use of special surface coatings or inhibitors. However there are technical hurdles to applying these processes to large structures in a continuous hydrogen environment. The current practice for using materials in hydrogen environments is to use exotic high-alloy steels. As these exotic materials yield a higher cost, tremendous savings may be realized by applying a cost-effective surface treatment to allow low-alloy steels to be used in a hydrogen atmosphere. Thus, it is desirable to determine a solution which

prevents hydrogen from permeating into the crystal matrix and/or reduces the deleterious hydrogen effects.

1.4. Residual Stress Benefits and Material Processing Techniques

Residual stress is introduced into material by mechanically or thermally inducing plastic deformation. After an external load is removed, the material returns to a state of internal force and moment equilibrium such that the "summation of the inelastic loading stress distribution and the elastic unloading stress distribution equals the remaining residual stress distribution with no external moment" [16, p246].

Work hardening or cold working are induced by straining a material above its yield point to induce plastic deformation. As a result, the tensile strength is increased and the ductility is typically decreased, allowing modification of material for a particular application [16]. Cold work is measured by a percentage and indicates the amount of material deformation induced.

Residual stress is also an important material factor. One fatigue cycle is described as the change from a stressed to an unstressed state. Fatigue life is described as the finite number of cycles a repeatedly cycled component experiences prior to failure. Designing residual stress into a component can increase fatigue life. Consider stressing a material above its designed specification which introduces a location of high stress above the yield point of the material. This highly stressed region can initiate cracks, potentially resulting in component failure. By strategically designing residual stresses into a

component, the original location of peak stress previously above the material yield point can now be lower than the material yield point, which reduces the potential for crack formation. This type of mitigation technique can be applied as a surface treatment for components with residual tensile stress remaining at the material surface. Thus applying a material processing technique which leaves the component surface under compressive residual stress, cracks that would have initiated do not propagate.

1.4.1. Shot Peening

Shot peening is a cost effective technique used to impart residual compressive stress in stainless and maraging steels, iron, aluminum, titanium, and nickel alloys [16]. Glass or ceramic shot, ranging in size from 0.18 mm to 3.35 mm, are accelerated with air pressure onto the material surface [17]. The beads impact and dimple the material which stretches in response. The bulk material provides resistance against the surface stretching, resulting in the formation of residual stress. The residual compressive stress induced by shot peening is through depths of 0.025 to 0.5mm [16]. The amount of plastic deformation induced from the shot peening process leaves a relatively high amount of cold work; at roughly 10% [18].

Shot Peening Benefits

The residual compressive stress introduced by shot peening is a proven technique for reducing environmental assisted cracking and stress corrosion

cracking [16]. Wilde, Shimada, and Chattoraj demonstrated that shot peening reduced the fraction of hydrogen absorbed and reduced the permeation of hydrogen through ASIS 4130 low alloy steel [19, 20, 21]. Furthermore, C.L. Ma et.al demonstrated that shot peening reduced the amount of environmental embrittlement in tensile tests of a Nickel-Silicone-Titanium alloy (Ni3(SiTi)) [22].

1.4.2. Laser Peening Background

Laser peening is a material surface treatment for improving fatigue life in components [22,24]. The concept is similar to shot peening except a laser is used to generate the material impacts. By using a short pulse laser to generate the shock wave, higher peak pressures can be generated which propagate deeper into the material leaving higher and deeper levels of residual compressive stress than shot peening with a lower amount of cold work [22]. Furthermore, the laser does not directly impact the material surface, leaving it more uniform when compared to other surface treatments such as shot peening.

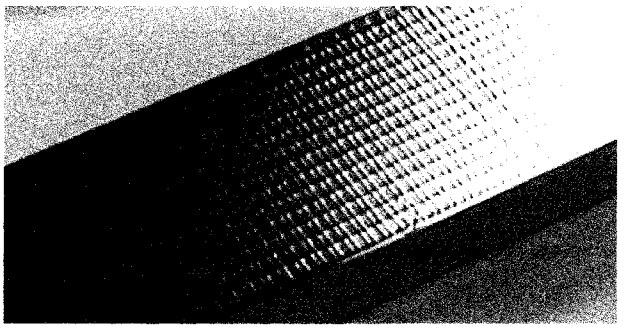

Figure 1 Laser Peened Surface.

Lasers used for laser peening typically have pulse durations on the order of tens of nanoseconds to reduce the heat transfer of the plasma into the material surface. A surface treatment that melts the material surface is undesirable as this affects the surface finish in addition to relieving some residual stress when the melted layer solidifies. Laser irradiances of roughly 10 GW/cm^2 are needed to generate pressure waves on the order of 10 GPa to plastically deform the material [2]. Indentations generated by the laser peening material displacement are typically between 10 μm and 20 μm deep.

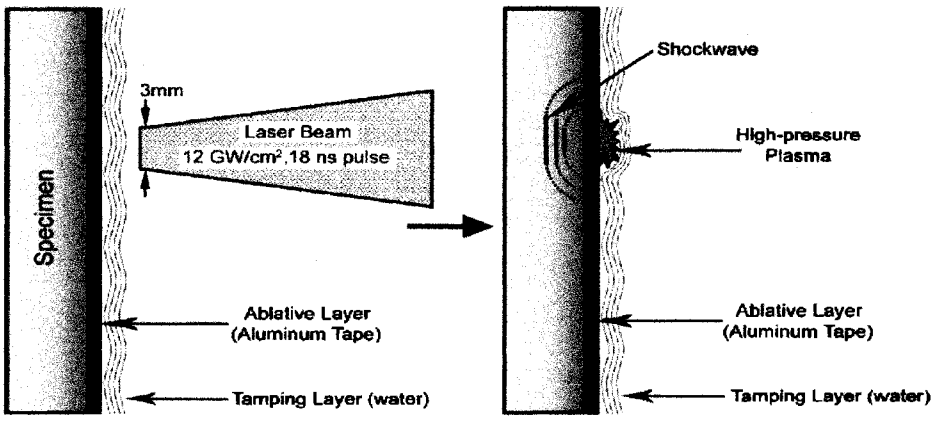

Figure 2 Schematic for the laser peening process before and after the laser shocks.

A planar shockfront dissipates slower compared to a spherical shockfront, and propagates deeper into the material surface allowing for greater depth of

compressive residual stress. Hence a higher energy laser provides a laser beam with a large footprint to generate a more planar pressure wave to propagate deeper into the workpiece. A 20 Joule pulsed laser can provide treatment size of roughly 3 mm x 3 mm at the material surface to generate the 10 GW/cm^2 power density needed to create a 10 GPa shock. Residual compressive stresses on the order of 1-5 mm deep are induced by laser peening systems meeting these high energy criteria [24].

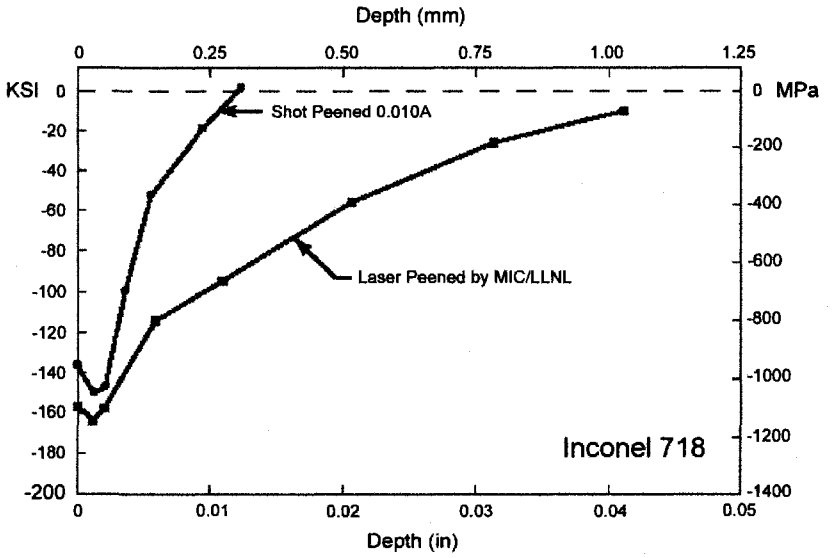

Figure 3 Residual stress vs. depth for shot peened and laser peened Inconel 718. Note the depth of compressive residual stress for the laser peened coupon is deeper than that for the shot peened coupon. Figure courtesy of Lloyd Hackel [25].

Benefits of Laser Peening for Stress Corrosion Cracking

A region of tensile stress typically remains along the base of a weld when

the weld solidifies and contracts. In susceptible materials, the area of tensile stress remaining around a weld base is referred to as the heat affected zone and can be prone to stress corrosion cracking.

The below Figure 4 demonstrates the stress corrosion cracking prevention in the heat affected zone of a laser peened weld. This stainless steel plate was welded, half laser peened, then corroded in a magnesium chloride solution [25]. Note the absence of cracking within the laser peened area (enclosed with a dotted white line). Laser peening changes the residual surface tensile stress of a weld heat affected zone to compressive residual stress which prevents cracks from propagating.

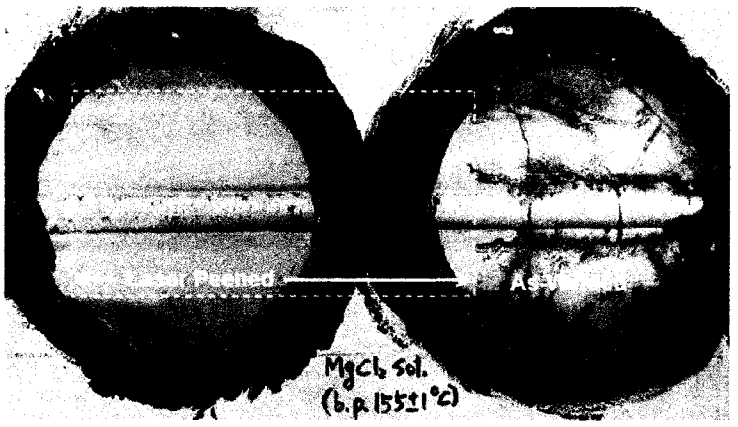

Figure 4 This 316L welded plate was laser peened then placed in 155° C of MgCl solution for 2 weeks. After removing from the solution, extensive cracking can be seen along and transverse the as-welded section. The cracks propagate along the weld toe and arrest at the boundary where the laser peened section begins. Photo courtesy of Lloyd Hackel [25].

In another test case to investigate laser peening benefits on existing cracks for materials used in power plants, corrosion test C-rings were pre-cracked and laser peened on one edge. After the laser peening, the Alloy 600 coupons were corroded in a dilute sodium thiosulfate solution (0.1 M at room temperature and pH of 3) for two days [26]. The material without pre-cracking generated new cracks in the solution. The material which was precracked then laser peened exhibited limited cracking while the precracked material without laser peening exhibited extensive cracking. This test demonstrated stress corrosion cracking required both tensile stress and a corrosive environment. Since the laser peening eliminates the residual tensile surface stress, it can be used as an effective treatment to prevent the formation and propagation of stress corrosion cracking.

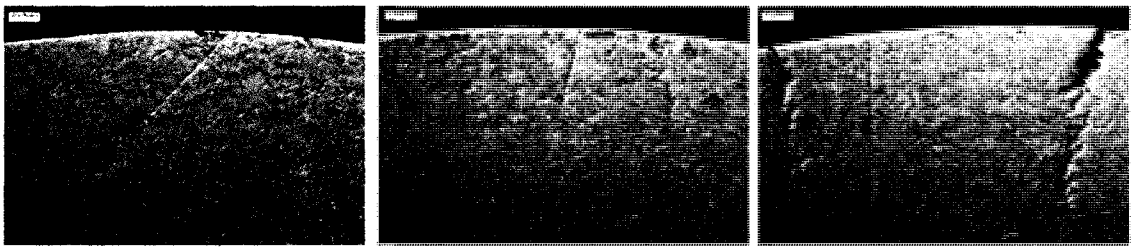

No pre-cracking, laser peened → No Cracking

Pre-cracked, then laser peened → Limited Cracking

Pre-cracked, no laser peening → Extensive Cracking

Figure 5 Alloy 600 U-bend specimens supplied from EPRI. Images courtesy of Hao-Lin Chen [26].

Benefits of Laser Peening for Fatigue Life

Previous studies demonstrate that laser peening can increase the fatigue life by an order of magnitude in metals [25, 26]. The introduction of surface residual compressive stress is an effective treatment to prevent fatigue cracks from propagating. The increased depth of residual compressive stress laser peening induces compared to traditional shot peening provides an additional fatigue life increase.

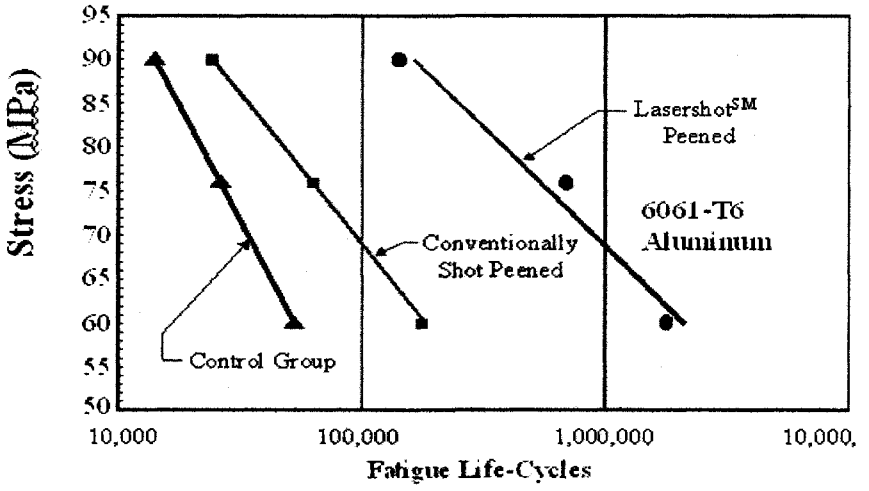

Figure 6 Fatigue life cycles in 6061-T6 Aluminum compact tension coupons tested at three stress levels. The laser peened samples demonstrate over a 10x fatigue lifetime improvement compared to the coupons which received no surface treatment and a significant fatigue lifetime improvement compared to the shot peened samples. Figure courtesy of Lloyd Hackel [25].

Material Effects of Laser Peening

A material dislocation is a discontinuity in the crystallographic structure

and can be located either within individual grains or along grain edges. Inelastic deformation as a result of stress or strain can cause the dislocation density to increase. Further fatigue cycling induces additional stress or strain and can cause the dislocations to rearrange within the crystal grain or along grain boundaries. Slip is a local effect of plastic strain and occurs within individual grains as shear deformation from dislocations moving along the crystallographic planes [16]. Slip bands form stress concentrations and can nucleate cracks. Other locations in material for cracks to nucleate include inclusions, corrosion pits, grain boundaries, and voids [16].

Independent work by El-Dasher and Peyre demonstrate that slip planes are introduced by the laser peening process in Ti-6-4 and 316L respectively [27, 28]. Although laser peening increases the dislocation density, it introduces less cold work when compared to shot peening [2, 28]. Smith et.al determined the amount of cold work introduced by laser peening Ti-6Al-4V to be from 6% to 12% increasing with the amount of laser peening layers used [29]. In contrast, Dane and Hackel measured the amount of cold work in laser peened Inconel 718 and Ti-6Al-4V to be from 1% to 2% [23, 25].

1.5. Hydrogen Charging Techniques

Hydrogen can be introduced into materials by various techniques: gaseous hydrogen charging, cathodic charging, or environmental charging. Cathodic and gaseous hydrogen charging were used in this study.

Thermal precharging using gaseous hydrogen exposes the material to pure

hydrogen gas at an elevated temperature and/or high pressure. The amount of time required to thermally precharge a material depends primarily on the hydrogen diffusivity of the material and the geometry of the test piece. Elevated temperature is used to increase the rate at which hydrogen diffuse into the material; decreasing the time to reach hydrogen saturation through the material bulk.

Cathodic hydrogen charging chemically introduces hydrogen to the test piece. Hydrogen ions generated in the solution are attracted to electrons in the metal test piece and permeate into the surface. Two hydrogen ions combine with an electron, forming an H_2 atom. The H_2 atoms then permeate into the material bulk and are attracted to low potential sites where they are energetically favored [4].

Environmental hydrogen charging can be accomplished with materials that have a high affinity for absorbing hydrogen and can be accomplished by exposing the material to a water or salt atmosphere. The water molecules react with the alloys in the material which break up the water molecule into oxygen and hydrogen gas. The hydrogen ions or gas is absorbed into the material [31].

1.6. Testing the Effects of Hydrogen

Measuring Total Hydrogen Content

Inert gas fusion is a measurement technique that is used to measure total hydrogen content in a material; sometimes referred to as LECO analysis after a prominent manufacturer of measuring equipment. The material is melted down

into a ceramic crucible and the hydrogen content is measured based on the gas fusion analysis principle [32]. This principle is based on heating a graphite crucible to temperatures exceeding 3000°C in an inert gas. A sample of known mass (usually 1 gram) is placed into the crucible where a water-cooled electrode above the crucible heats and melts it. The hydrogen in the sample is emitted as hydrogen gas (H_2) which is carried out by the carrier gas (usually Argon) to the detectors.

The detectors are typically thermal-conductivity detectors (universal detectors) that respond to the thermal conductivity of a carrier gas. The sensitivity of the measurement depends on the difference in thermal conductivity between the carrier gas (in this case Argon) and the gas to analyze (Hydrogen). The detector cannot discern the types of gases in the carrier gas, so the other gases such as Nitrogen (N_2), CO, and CO_2 must be removed. This is accomplished by passing the gas first over a reagent to convert the CO to CO_2, and then over a medium which absorbs the CO_2. The N_2 is then removed by passing the sample stream through a long column. The lighter H_2 gas exits the column first followed by the N_2 gas. The measurement of the total H_2 content is made on the first exit of gas from this tube. To determine the hydrogen content, the sample is compared to calibrated samples with known hydrogen concentrations [32].

The samples need to have surface contaminants removed prior to placing in the crucible for analysis. Prior to placing in the chamber the samples are filed, rinsed with acetone, and dried with warm air.

Microstructure

A Scanning Electron Microscope (SEM) uses a tungsten or lanthanum cathode to generate electrons. The electrons are rastered across a surface where the secondary electrons dislodged from the sample are detected by a positively charged grid. This method of imaging can resolve features in the nanometer range. An SEM can also be used to determine the chemical composition of a material. As the secondary electrons are removed from the sample surface, they emit X-Rays which can be used to determine the chemical composition.

A Transmission Electron Microscope (TEM) uses a tungsten filament to generate an electron beam in vacuum that is narrowly focused on a very thin slice of sample material. The electrons that pass through the sample are imaged by a phosphor screen, CCD, or film. Less electrons are transmitted to the screen where the sample has more density and more electrons are transmitted to the screen where the sample has less density. This type of imaging can resolve features to 0.2 nm.

Material Properties: Microhardness, Tensile Strength, and Ductility

Materials are characterized by their microhardness, tensile strength, and ductility [33, 34]. Materials susceptible to hydrogen embrittlement demonstrate a decrease in ductility in addition to a potential increase in yield strength. This increases the susceptibility to cracking and can decrease the fatigue life.

Microhardness

Microhardness testing is a cost effective measurement which uses a diamond brale penetrator at a calibrated load to push and displace material [35]. The size of the residual indentation is measured and the hardness of the material is then inferred. To measure the microhardness of a material through the depth, the test piece is cut perpendicular to the surface and polished. A step-scan of microhardness dents are generated across the sample cross-section.

Balasubramanian proposed that hydrogen diffusion can be estimated from microhardness measurements. Other studies have utilized this method in calculating the hydrogen diffusivity in materials such as Al-Li alloys, austenitic stainless steels, and iron aluminides [33, 37].

From Porter, Fick's second law of diffusion states [38]:

$$\frac{\partial C_H(x,t)}{\partial t} = D_H \frac{\partial^2 C_H(x,t)}{\partial x^2} \qquad (1)$$

Where C_H is the hydrogen concentration at depth x (μm) and time t (s). D_H is the diffusivity in units of length^2 * time^{-1}. Solving equation (1) with the boundary conditions $C_H(x=0,t)=C_S$ and $C_H(x,t=\infty)=C_b$ with C_S being the concentration at the surface and C_b being the concentration of the bulk:

$$C(x,t) = C_s - (C_s - C_b)erf\left(\frac{x}{2\sqrt{D_H t}}\right) \qquad (2)$$

Four assumptions are made to relate (2) to microhardness. First, the

variation of microhardness from the surface to the bulk is due to hydrogen and second, the material has no microhardness variation with depth [33,37]. Third, ($C-C_b$) is proportional to the increase in microhardness over the bulk through the diffusion zone [33,37]. Fourth, the diffusion coefficient is constant with time. With these assumptions and by rearranging (2) and equating with (1), a correlation between diffusivity and microhardness increase can be as follows [33,37]:

$$\frac{C(x,t)-C_b}{C_s-C_b}=\frac{MHv(x,t)-MHv_b}{MHv_s-MHv_b}=1-erf\left(\frac{x}{2\sqrt{D_H t}}\right) \tag{3}$$

Hence diffusivity can be inferred from the microhardness measurement. Note however that these equations do not account for the effects of residual stress, which also changes the diffusivity of a material. In an elastic stress field this equilibrium hydrogen concentration can be expressed as [36]:

$$c = c_0 \exp(\sigma V_H/RT) \tag{4}$$

Where c0 is the equilibrium hydrogen concentration in an unstressed lattice, σ is the hydrostatic stress, VH is the partial molar volume of hydrogen, R is the universal gas constant, and T is temperature in Kelvin. The first assumption in the above analysis assumes the microhardness variation is due solely to hydrogen, however laser peened materials show a microhardness variation due

to the residual stresses [42]. Thus microhardness measurements alone are not sufficient to make a comparison of the hydrogen effects in metals which contain residual stresses due to laser peening.

The location of the change in residual stress from compressive to tensile or from tensile to compressive can be inferred by a microhardness profile since compressive stress increases the local hardness while tensile stress decreases it. Hence the change from compressive to tensile residual stress can be inferred by noting the corresponding change in microhardness profile from the material bulk. This provides an estimate for the depth of residual compressive stress by analyzing the microhardness profile.

Yield Strength

Yield Strength is measured using tensile specimens which are typically round or rectangular bars axially pulled by a hydraulic machine at a known rate. The stress and strain of the system is recorded as the specimen plastically deforms and ultimately breaks. Material properties can be determined from the resultant stress-strain plot. The yield point of the material is determined at the "first stress in a material, less than the maximum obtainable area, at which an increase in strain occurs without an increase in stress" [35]. The yield point of the material is determined at a defined offset from the point where the stress of the material deviates from the stress to strain linear trace, typically expressed as an offset of 0.2%. The tensile strength is the maximum load the specimen.

Ductility

The parameters used to quantify the tensile ductility of a material are elongation at fracture (Elu) and reduction of area (RA). The reduction of area is the change in the load-bearing cross-sectional area at fracture normalized by the initial cross-sectional area, defined by equation (5). Elongation at fracture is the percentage increase in length of the coupon during the test, defined by equation (6). Lower values of elongation and reduction of area indicate lower ductility.

$$RA = \frac{-\Delta A}{A_i} = \frac{A_i - A_f}{A_i} = 1 - \frac{A_f}{A_i} \tag{5}$$

$$El_u = \frac{\Delta L}{L_i} = \frac{L_f - L_i}{L_i} = \frac{L_f}{L_i} - 1 \tag{6}$$

Performance (Fatigue, Crack Growth)

The fatigue performance of a material can be quantified from fatigue life and fatigue crack growth rates. Fatigue life is the number of cycles a material experiences prior to cracking for a given load and is defined in this study as the amount of cycling until 10% compliance. Fatigue crack growth is commonly reported as the rate at which a crack propagates in a material (da/dN) as a function of the difference in stress intensity factor (ΔK) (often referred to as da/dN vs. ΔK curves). Fatigue life tests determine the number of cycles to nucleate and propagate a crack to failure under a constant cyclic stress, while crack growth rate testing determines the rate of crack propagation as a function of loading conditions (described by the difference of stress intensity factor). Prior fatigue testing in laser peened materials show a typical 10x improvement in fatigue life

[25]. Previous crack growth testing performed with Ti-6Al-4V demonstrate a 10x reduction in crack growth rate due to laser peening [40]. These improvements can be attributed to the compressive residual stress at the material surface which prevents fatigue cracks from propagating.

To examine the effects of hydrogen on material performance, the materials need to be either tested in a hydrogen filled chamber or precharged with hydrogen and tested in air. The latter technique was used in these experiments as fatigue tests in high-pressure hydrogen gas are particularly difficult to execute.

2. CONTENT

2.1. Material Processing Technique

Treatment spot size and higher repetition rate directly influence the processing time of the material. Hence a high energy per pulse with high repetition rate laser was desirable for this study. The laser used in this study was capable of treating surfaces at a rate of 0.19 m^2 per hour with an irradiance of 10 GW/cm^2 and a pulse duration of 18 nS.

Laser Description

The laser used in this research was a Master Oscillator Power Amplifier (MOPA) design capable of producing 25 J pulses of 1053 nm light at 18 nS with a repetition rate of 6 Hz. The oscillator consisted of a flashlamp pumped Yttrium Lithium Fluoride (YLF) rod in a q-switched ring cavity. The oscillator output was typically 12 mJ at 25 nS. The oscillator output was magnified and propagated into a two pass 9 mm YLF pre-amplifier with a typical output of 350 mJ. The Gaussian beam was expanded and overfilled onto a 22 mm square mask. This square bean was again expanded through an anamorphic telescope which optically expanded the square beam to a 10 mm x 100 mm tall rectangular beam. The beam then entered the main amplification section of the laser system, where it passed a total of eight times through a Nd doped phosphate glass slab. Each pass through the main glass amplifier ran in a zig-zag configuration to evenly distribute the energy into the beam, reducing the birefringence due to the thermal gradient across the face of the slab. The glass slab was cooled with 60 gpm of

deionized water to remove heat from the flashlamps. After amplification through the first half of the main amplifier chain, the beam was sent to a phase conjugation cell to reduce the wavefront distortion caused by glass irregularities and residual thermal birefringence from the glass slab. The passive wavefront correction system used Stimulated Brillion Scattering to generate a diffracted beam with a wavefront phase reversed from the incoming beam. The wavefront reversed beam propagated again through the amplifier system, picking up all the phase errors in reverse, canceling them out. The result was a nearly uniform "top hat" spatial profile beam [41].

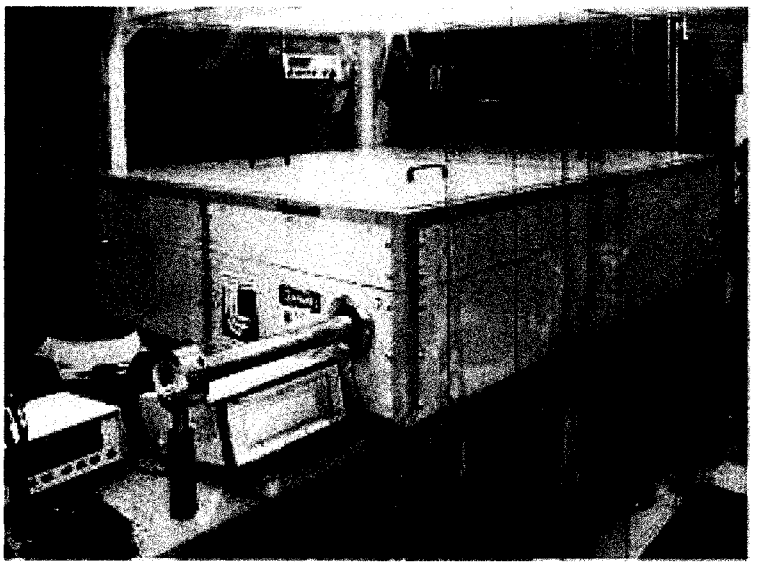

Figure 7 The LLNL Laser Peening System.

The laser output was sent through relay optics to image the beam in the treatment area. The laser output was stationary and two six-axis robots were

used for the manipulating of coupons for treatment.

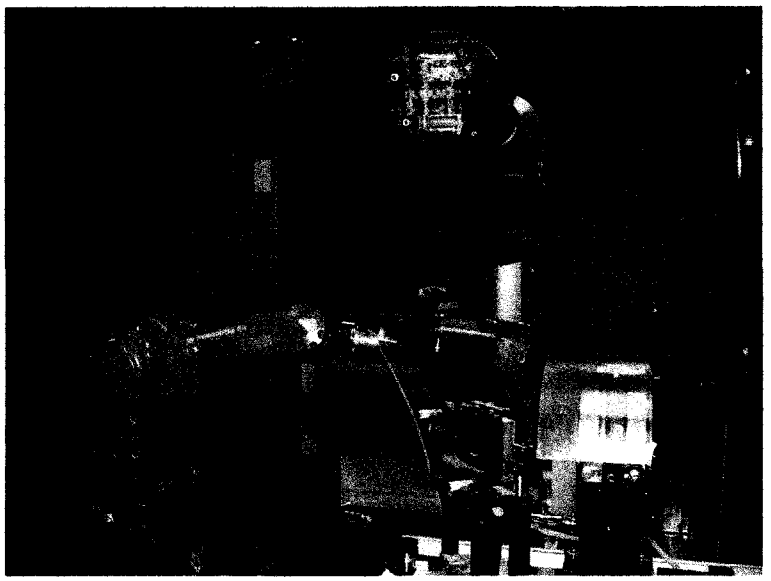

Figure 8 LLNL laser peening treatment area. Six-axis robotics were used for maneuvering coupons for treatment. Note the use of sound absorbing material on the back walls. The laser peening treatment generates >130 dB sound pulses as the shockwave propagates through the material.

2.2. Previous Work

In a previous study, Hill and Liu investigated the effects of laser peening on hydrogen charged 316L stainless steel coupons by performing microhardness measurements. The coupon hydrogen charging conditions and microhardness measurements are summarized here for convenience [42]. This study used the coupons provided by Hill and Liu to perform a series of SEM images through the coupon depth.

Electrolytically Hydrogen Charged 316L from Hill and Liu [42]

Hill and Liu tested hydrogen effects in laser peened 316L stainless steel; the conditions tested in that study are summarized in Table 1. Two coupons; 316L as-received and 316L laser peened were electrolytically charged with hydrogen. The as-received and laser peened specimens (316-HC and 316-LP+HC) were cathodically charged in a four-port electrochemical cell of aqueous 5% H_2SO_4 at room temperature. To maintain constant temperature, the setup was partially immersed in a Dow Corning 200 silicone oil bath in a thermostat unit. A Luggin probe positioned the Ag/AgCl reference electrode in a water jacket away from the test solution and a platinum counter electrode controlled by a precision power supply providing a constant, uniform exchange current density of 10m A/cm^2 over the 144 hrs of charging duration. An aerater purged the test solution with gas or air and a condenser column kept the bath from evaporating. The specimens were suspended in the solution through the larger central port.

Table 1 Coupon treatments and labels used in the 316L study.

Coupon Label	**316L Treatment**	**Label**
1	As-Recieved Material	316-AR
2	Laser peened	316-LP
3	No surface treatment, hydrogen charged	316-HC
4	Laser peened then hydrogen charged	316-LP+HC

A Leitz Wetzlar Metallix 3 Vickers Microhardness Tester was used for profiling the subsurface microhardness (Mhv) of the four coupons. The machine

was equipped with a diamond indenter and an optical microscope with 500x magnification. The coupons were sectioned in half and polished to expose the cross-section. An indentation load of 100 gf was applied over 10 seconds for each indent. The diagonals of each indent were measured using the attached microscope and the microhardness values were calculated from the following formula [42]:

$$MHv = \frac{2000P\sin(\alpha/2)}{d^2} = \frac{1854.4P}{d^2} \tag{7}$$

Here P was the applied load, α was the face angle of the indenter (136°), and d was the diagonal size of the indentation (μm).

The results of the microhardness profiles are displayed in Figures 9 through 13. The as-received coupon showed a uniform increase in hardness by roughly 30 MHV.

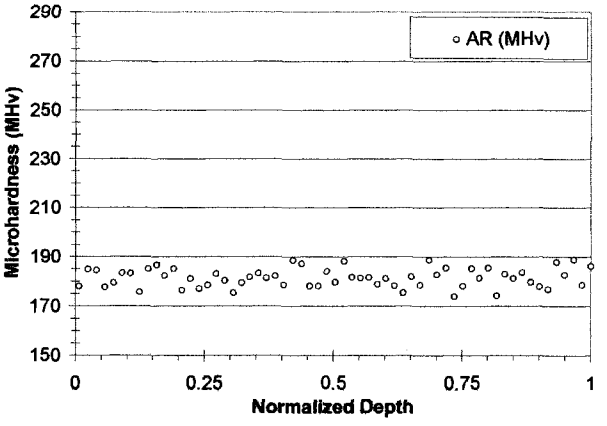

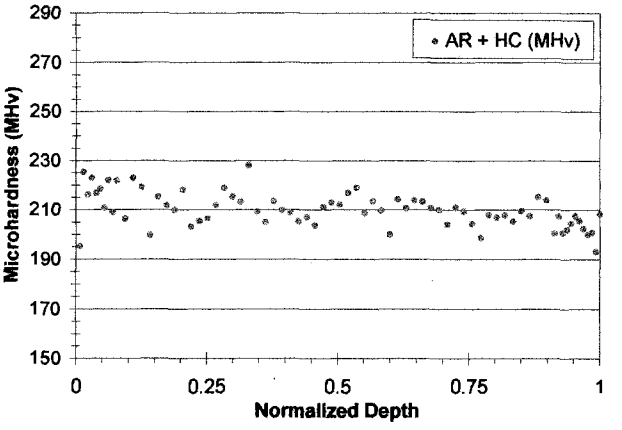

Figure 9 Left - Microhardness profiles for the 316L coupon without hydrogen charging. Data courtesy of Kevin Liu and Mike Hill [40].

Figure 10 Right - Microhardness profiles for the 316L coupon witht hydrogen charging. Data courtesy of Kevin Liu and Mike Hill [40].

In comparison, the laser peened sample (Figures 11 and 12) demonstrated a non-uniform microhardness across the normalized thickness. This was not unusual as the stress distribution varies across the thickness of the sample. The laser peening induces a compressive stress at the surface which increases the surface hardness, while the tensile region at the center produces a decrease or no change in the microhardness [34, 42]. Of interest to note in these results was the minimal difference in microhardness between the laser peened samples with and without hydrogen charging.

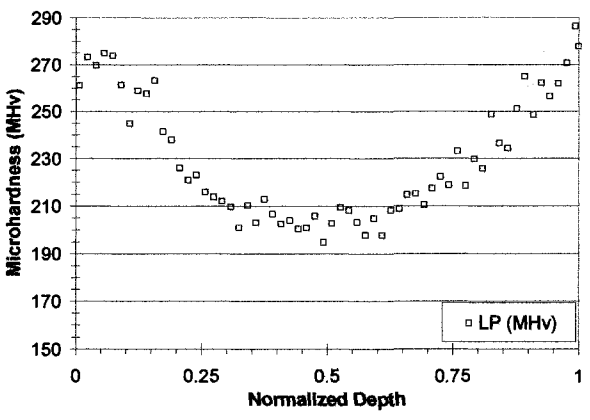

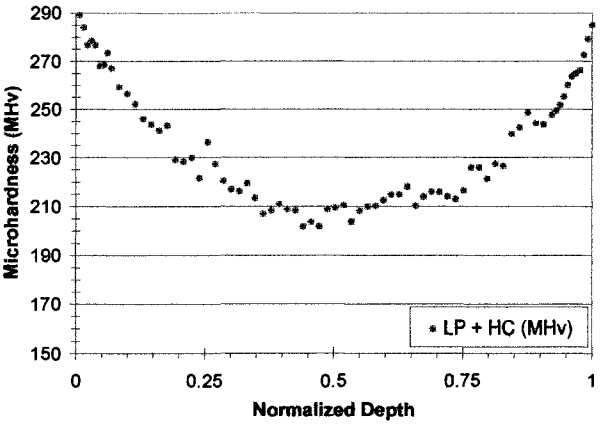

Figure 11 Left - Microhardness profiles for the 316L laser peened coupon without hydrogen charging. Data courtesy of Kevin Liu and Mike Hill [40].

Figure 12 Right - Microhardness profile for the 316L laser peened coupon with hydrogen charging. Data courtesy of Kevin Liu and Mike Hill [40].

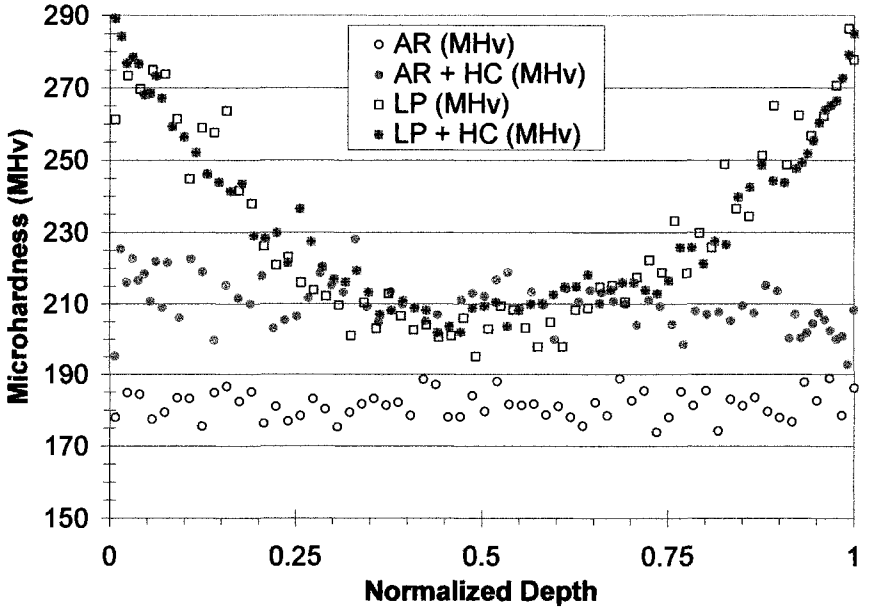

Figure 13 Microhardness profiles for 316L coupons, all tested conditions. Data courtesy of Kevin Liu and Mike Hill [40].

2.3. Microstructure Analysis in 316L

The 316L electrolytically charged coupons provided by Hill and Liu were polished and analyzed using SEM. Images were taken of coupons with cathodic charging, laser peening, and laser peening with cathodic charging (samples 316-HC, 316-LP, and 316-LP+HC).

In the as-received hydrogen charged coupon, some subsurface voids were seen, but no major cracking observed.

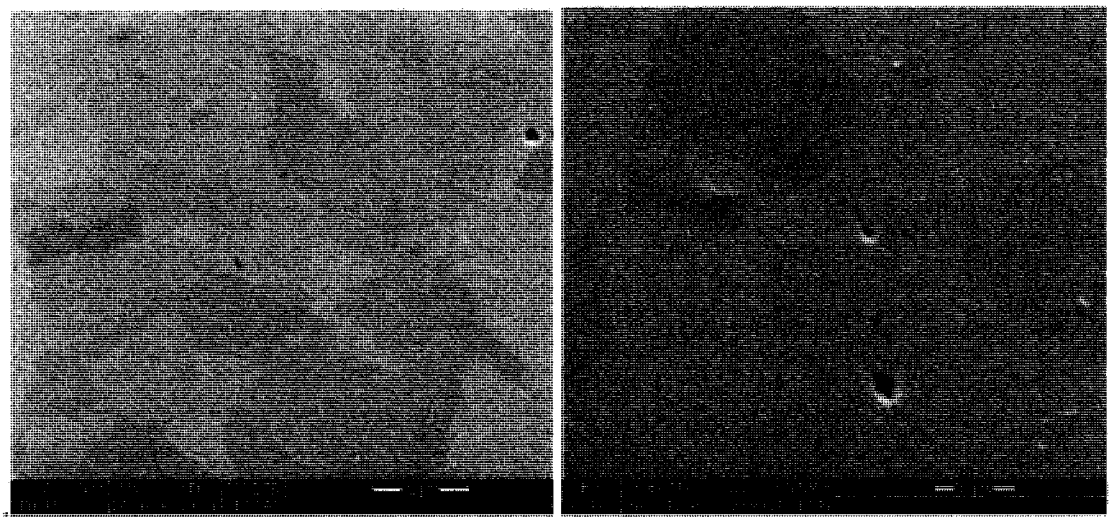

Figure 14 Left - SEM image for the electrolytically charged 316L coupon bulk with no surface treatment.

Figure 15 Right - SEM image for the electrolytically charged 316L coupon bulk with no surface treatment.

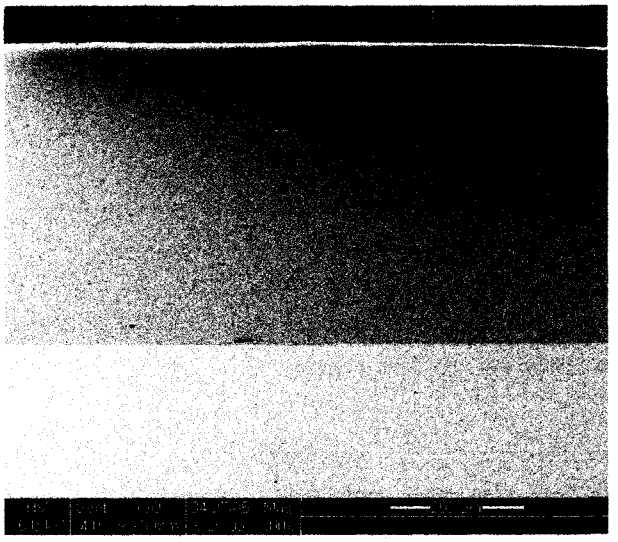

Figure 16 SEM image of the 316L laser peened coupon with no cathodic charging.

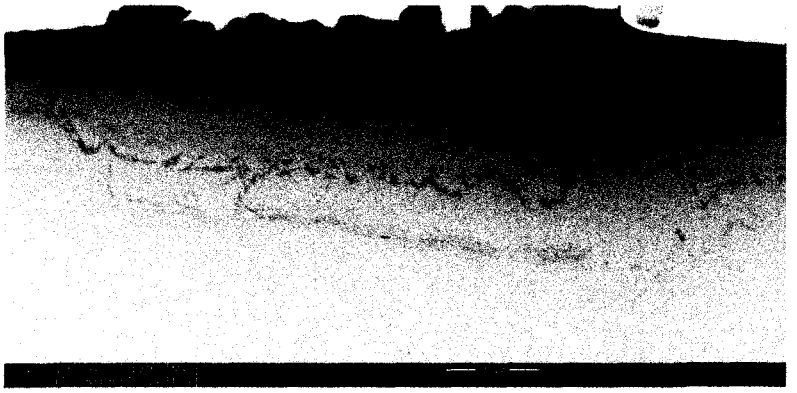

Figure 17 Closeup of a crack in laser peened coupon with no cathodic charging.

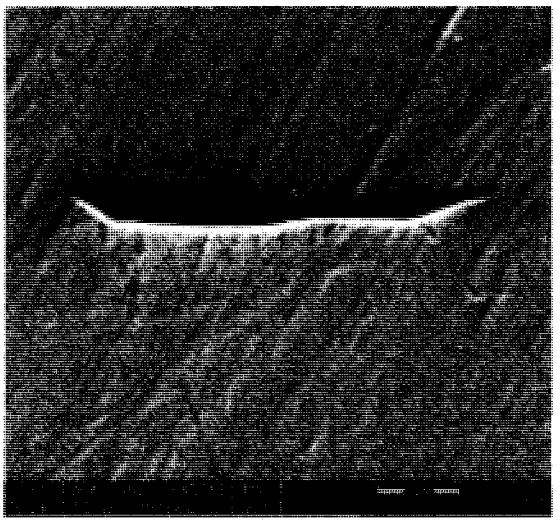

Figure 18 SEM image for 316L laser peened coupon with no cathodic charging. This crack was typical of those found subsurface in the laser peened material. It is approximately 25 μm long and runs parallel to the coupon surface.

SEM images of the surface and bulk of the laser peened then cathodic charged coupon showed frequent cracking (Figures 19 through 22). The laser peened sample with no cathodic charging had subsurface cracks typically 50 μm in length and parallel to the coupon surface. The laser peened then cathodically charged sample had a higher frequency of larger cracks. These cracks were also parallel to the coupon surface but were typically longer at roughly 150 μm, one was found longer than 600 μm.

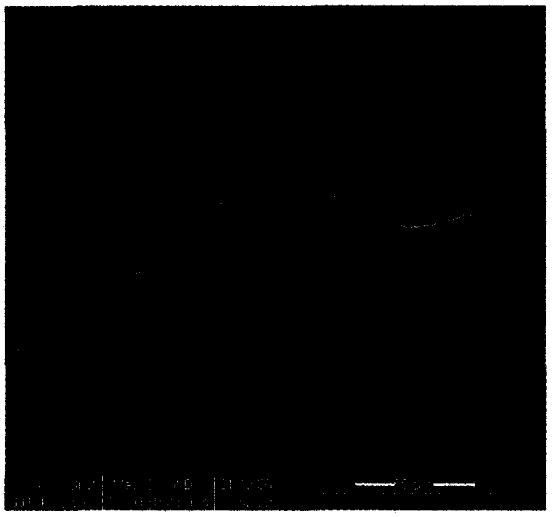

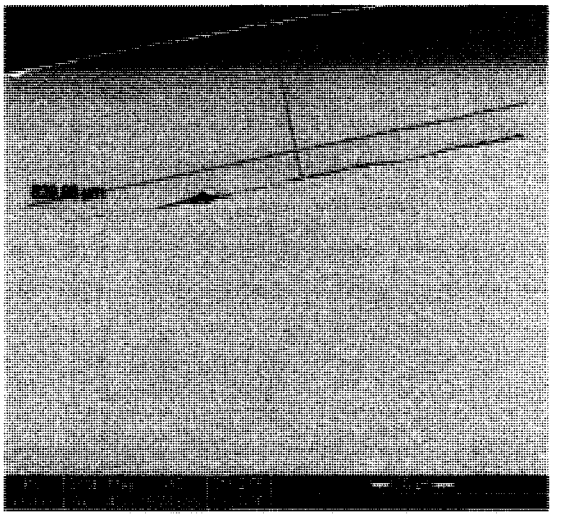

Figure 19 Left - SEM image in the bulk of the 316L laser peened coupon with cathodic charging.

Figure 20 Right - SEM image near the surface in the 316L laser peened coupon with cathodic charging.

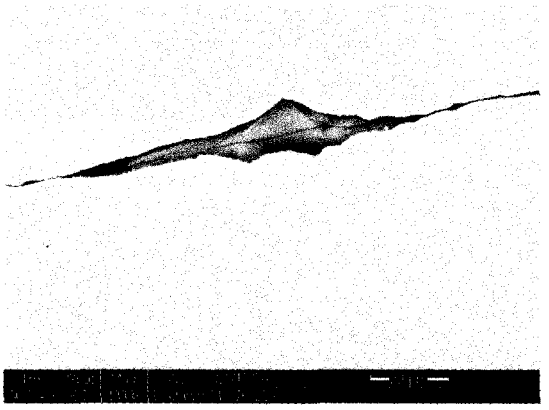

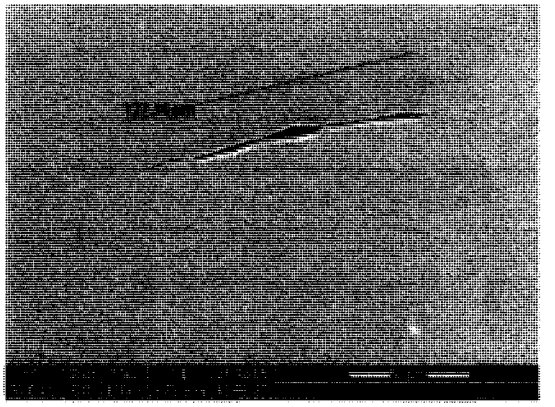

Figure 21 Left - SEM image of subsurface cracks in the laser peened coupon with cathodic charging.

Figure 22 Right - SEM image of subsurface cracks in the laser peened coupon with cathodic charging.

The hydrogen tends to collect along grain boundaries and voids, locations the areas of lower energetic potential [9, 31]. The voids coalesce and push against the surrounding material, causing stress and thereby increasing the local microhardness. Once a threshold is reached a crack extends, locally reducing the stress. This could explain why the laser peened material had a minimal increase in microhardness and had a higher frequency of subsurface cracking in the hydrogen charged specimens.

2.4. Tensile Coupon Tests

Three materials were evaluated in the tension study: Nickel-based Alloy 22, iron-based precipitation-strengthened austenitic stainless steel A286, and nitrogen-strengthened austenitic stainless steel 21-6-9.

Nickel-based Alloy 22 was chosen for the amount of data available in literature, ease of obtaining material, and it has been previously optimized for laser peening parameters. Stainless steel 21-6-9 was chosen for the substantial hydrogen-assisted fracture data available in the literature and for the ease of obtaining material. This material (in the forged condition) demonstrates a loss in ductility of roughly 35% after hydrogen precharging [43]. However, this material had not been previously characterized for optimal laser peening parameters. Stainless steel A286 displays approximately a 50% loss of reduction in area after hydrogen precharging [44]. Similar to 21-6-9 and alloy 22, A286 exhibits good corrosion resistance; however, A286 has a tendency to exhibit weld cracking, thus it could benefit from a laser peening type treatment [45]. As with the 21-6-9

steel, the A286 material had not previously been characterized for optimal laser peening parameters.

Table 2 Nominal composition (wt%) of the alloys used in this study. Alloy 22 plate material was supplied in the annealed condition in conformance to ASTM B-575-97, 21-6-9 was supplied as 2.5" diameter round, annealed bar; and A-286 was supplied as 6" diameter round bar in the peaked-aged condition (solution annealed at 900° C for 2 hr, then aged 720° C for 16 hr).

	Fe	Ni	Cr	Mn	Mo	W	Si	Co	V	C	N	P	S	others
Alloy 2 plate (UNS N06022)	3.8	Bal	21.8	0.34	13.0	3.0	0.08	0.5	0.18	0.002	nr	nr	nr	—
21-6-9	Bal	6.5	19.5	8.9	nr	nr	0.64	nr	nr	0.037	0.27	0.014	0.0016	—
A-286	Bal	24.33	13.91	0.11	1.18	nr	0.20	0.13	0.24	0.04	nr	0.017	0.001	2.05Ti 0.008B

ASTM E8 subsized rectilinear tensile bars were machined from the alloys (Figure 24). The specimens were extracted parallel to the axis of the bar using Electro-Discharge Machining (EDM) with a square gauge section of 6.4 mm x 6.4 mm. The specimens were laser peened on all sides, including the grip sections and ends. The coupons were treated at 10 GW/cm^2 using an 18 nS pulse width and two layers of treatment. A spray coating of approximately 40 μm

was applied as the ablative layer. This ablative layer was reapplied for each layer of laser peening treatment.

Table 3 Laser parameters used for the tensile coupon study.

Parameter	Value
Irradiance	10GW/cm^2
Pulse Width	18ns
Laser energy	16.2J
Treatment spot size	2.9mm x 3.1mm
Ablative layer	Black paint
Treatment layers	2

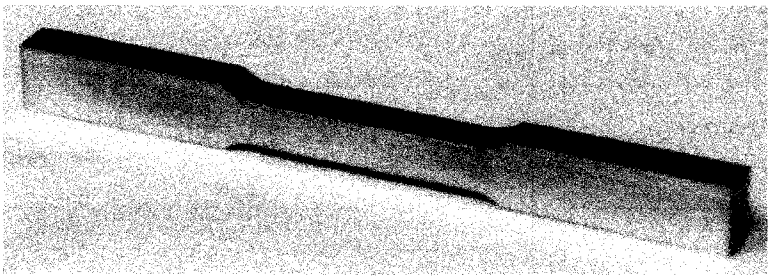

Figure 23 Flat tension coupon.

The Laser Peening Process

The coupons were first cleaned by cloth using acetone and again by cloth using Ethanol. The ablative layer spray coating was carefully applied such that no air was trapped between the ablative layer and the coupon surface. The coupons were placed in a fixture designed to hold the coupons in a repeatable

fashion. The fixture was moved into the corresponding laser image plane using a six axis robot (Figure 8). The robot was timed with the laser pulse triggers to move to the next treatment location prior to each laser shot.

After the first treatment, the ablative layer was removed and cleaned again by acetone followed by ethanol. A new ablative layer was applied for the next layer of laser peening treatment. Each peening layer was offset with respect to the previous layer. For example, with two layers of laser peening, the second layer was offset in both directions by 50% of the treatment spot size to insure uniform coverage. In some cases 3 layers of treatment were used. For three layers of treatment each layer was offset 33% in both directions. The robotics were programmed such that the orientation of the coupon was almost normal to the incoming laser beam with a small horizontal tilt to minimize the back-reflection off the surface part from damaging the delivery optics. For complicated geometries such as the tensile coupons treated here, a code was developed in MatLab to generate a mesh pattern for the treatment. In addition to treating all the "flat" sides of the coupon, laser pulses were applied at the coupon edges at a 45° angle measured from the coupon radial axis to insure the coupon corners were also receiving compressive stress. This type of absolute coupon coverage was necessary in the event that the hydrogen permeated at different rates through the as received and laser peened surfaces.

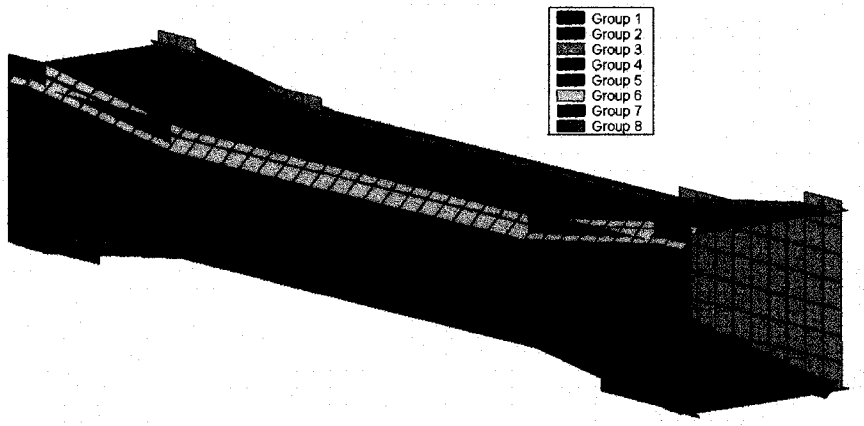

Figure 24 Peening pattern for the tensile coupon. Each square represents one laser spot.

Laser Calibration

All laser peening was performed in conformance to the Aerospace Material Specification 2546 [46]. To insure the laser imparted the correct amount of residual compressive stress, a calibration using an Almen C strip was performed prior to treating each coupon. Almen C strips were made of SAE 1070 cold rolled spring steel and when laser peened with one layer at 10 GW/cm^2, 18 nS the treated surface elongats causing the strip to curve [46]. The curvature induced was .010" ± .001" and was used as a reference to insure the water and laser parameters were appropriately set.

After the coupons were treated (half with laser peening and half taken in the as-received condition) they were precharged with hydrogen. The coupons were precharged with138 MPa hydrogen gas at 300° C for 34 days to saturate.

After charging they were stored at 253 K until testing, less than 3 days. Prior to testing the specimens were warmed to room temperature. The broken specimens were also stored at 253 K to prevent hydrogen outgassing.

Table 4 Sample labels and test conditions for the tensile coupon study.

Test Condition	**Treatment**	**Alloy 22 Labels**	**21-6-9 Labels**	**A286 Labels**
AM	As-Recieved Material	AM-1, 2	AM1, 2, 3	AM-1, AM-2
LP	Laser peened	Al1, AL2, C13, C14, 15	S3, S6, S9	A1, A3, A6
AM + HC	No surface treatment, hydrogen precharged	C2, C5, C6	S4, S7, S8	A7, A8, A9
LP + HC	Laser peened then hydrogen precharged	C1, C3, C4	S1, S2, S5	A2, A4, A5

2.4.3. Total Hydrogen Content

The witness samples (26 mm long and 6 mm in diameter), as well as approximately 6 mm thick pieces cut from the grip sections of the tensile specimens, were sent to a commercial testing laboratory for hydrogen analysis by hydrogen extraction (LECO Technical Services Laboratory). The hydrogen content after thermal precharging was found to be the same for the as-received and laser peened specimens (Table 5). These hydrogen contents were consistent with previous studies on similar alloys [47].

Table 5 LECO hydrogen content results; AM = as-received, LP = laser peened, HC = hydrogen-precharged.

Material	Specimen ID	Condition	H-content (wt ppm)
Alloy 22	C1c	LP	110
	C2c	AM	110
	C3	LP	110
	C5	AM	110
21-6-9	S1c witness	LP + HC	210
	S3c witness	AM +HC	210
	S5	LP + HC	220
	S8	AM + HC	220
A-286	A5	AM + HC	110
	A9	LP + HC	110

The time to reach hydrogen saturation for the thermal precharging conditions and the specimen geometry was estimated to be approximately 30 days, using the Sandia National Laboratory diffusion code called DIFFUSE [48, 49]. Compressive stress, such as that imparted by the laser peening process, reduces the equilibrium hydrogen content in metals and can change the rate of hydrogen diffusion. However, the magnitude of change in hydrogen content and hydrogen diffusion was estimated to be small in steels for reasonable residual stresses. The results presented in Table 5 support this interpretation as there

was no difference in hydrogen content between the as-received specimens and the laser peened specimens.

2.4.3. Microhardness Measurements

Microhardness measurements in Figure 25 for Alloy 22 demonstrated a slight increase in the laser peened precharged coupon compared to the as-received precharged coupon. The microhardness increase for the laser peened precharged coupon above the bulk value of roughly 243 MHv extends to a depth of roughly 1.5 mm deep in the material. This depth corresponds to typical depths of compressive residual stress for previously treated Alloy 22 [24].

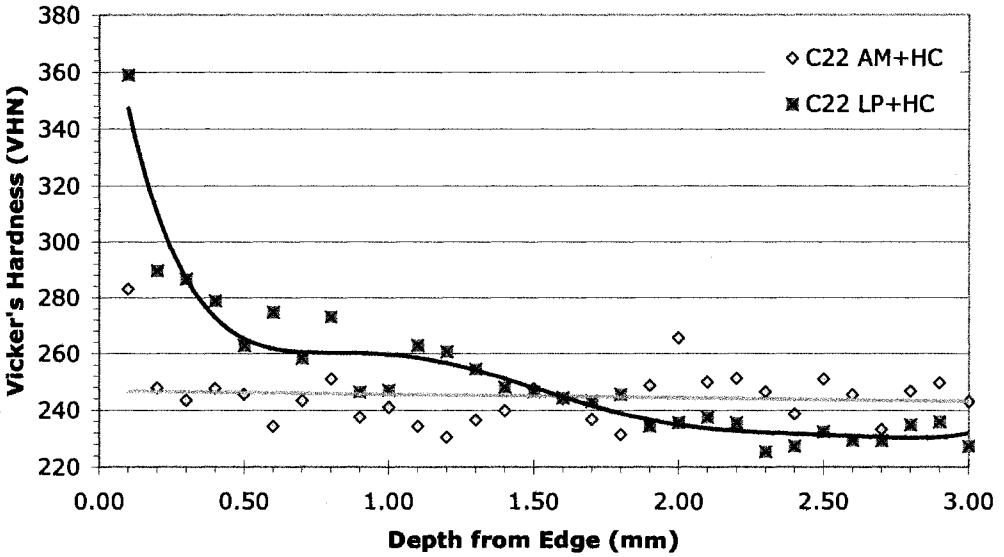

Figure 25 Alloy 22 microhardness profiles for both the as-received precharged and the lase peened precharged coupons.

The 21-6-9 material microhardness measurements in Figure 26 show a

slight increase in microhardness for the laser peened precharged coupon compared to the as-received precharged coupon. The microhardness for the laser peened precharged coupon is above the bulk microhardness value of roughly 240 MHv to a depth of 0.8 mm. Existing laser peened literature in the 21-6-9 material could not be found for comparison, thus a compressive residual stress to a depth of roughly 0.8 mm demonstrated the laser peening treatment had an effect on the material.

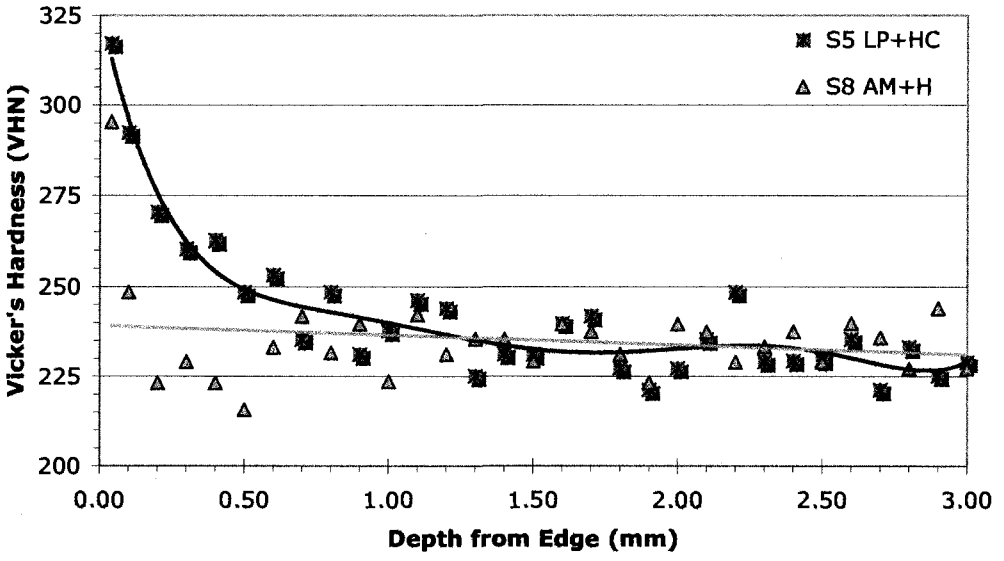

Figure 26 Microhardness profiles for 21-6-9. A linear fit was applied to the as-received precharged coupon and a polynomial fit was added to the laser peened precharged coupon to guide the eye.

The A286 material microhardness measurements in Figure 27 also show a small increase in microhardness for the laser peened precharged coupon

compared to the as-received precharged coupon. These results were similar to those for the 21-6-9 material as there was an increase in microhardness for the laser peened precharged material to a depth of roughly 0.8 mm.

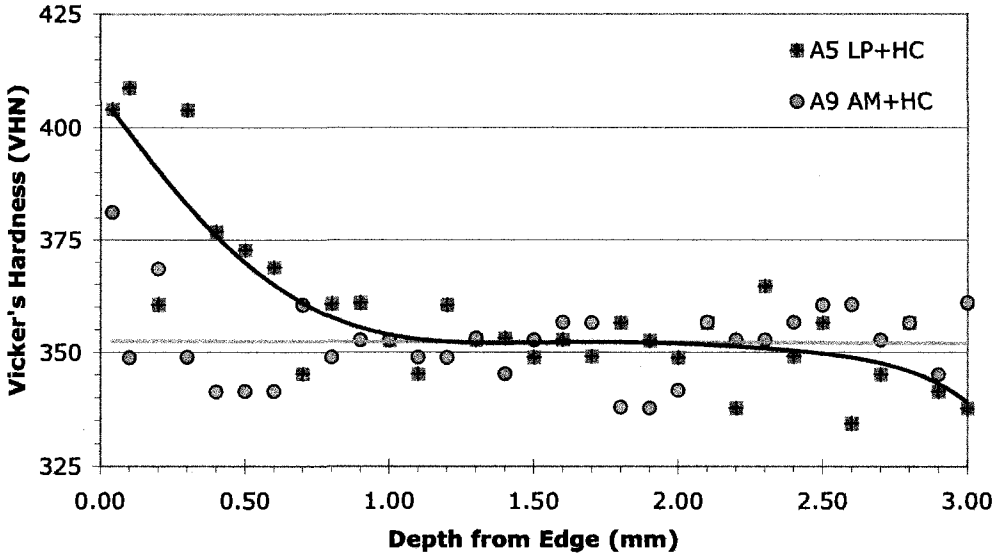

Figure 27 Microhardness profiles for A286. A linear fit was applied to the as-received precharged coupon data and a polynomial fit was added to the laser peened precharged coupon data to guide the eye.

2.4.3. Tensile Testing Results

All specimens were tested on a servo-hydraulic testing machine (MTS 810). A knife-edged extensometer with a gauge length of 12.7 mm (0.5 inch) was used for strain measurements during tensile testing. Testing was performed at a constant displacement rate corresponding to a strain rate of approximately 1.8x10-3 s-1 (in the plastic regime prior to necking). The yield strength (0.2%

offset, Sy) and tensile strength (maximum engineering stress, Su) are reported as well as the uniform elongation (engineering strain at maximum load, Elu) and total elongation (engineering strain at failure, Elt). Two or three specimens were tested for all conditions.

The reduction of area was determined from the geometry of specimen's cross section at fracture and the original cross section. The ductility parameters with and without hydrogen were also reported as follows:

$$RRA = \frac{RA(\text{H} - \text{precharged})}{RA(\text{non} - \text{charged})} \tag{8}$$

$$REl_u = \frac{El_u(\text{H} - \text{precharged})}{El_u(\text{non} - \text{charged})} \tag{9}$$

Tensile Results for Alloy 22

Figures 28 and 29 display the tensile flow curves for the Alloy 22 material. Both the as-received and laser peened coupons demonstrated a loss in ductility due to the hydrogen precharging. The as-received material exhibited less reduction in uniform elongation (RElu calculated from equation 9) of 0.90 when compared to the laser peened RElu of 0.64. The as-received material demonstrates an RRA (calculated from equation 8) due to hydrogen precharging of 0.6 while the laser peened coupon demonstrated an RRA due to hydrogen precharging of 0.4. Thus when exposed to hydrogen precharging the as-

received Alloy 22 material retained more of its initial ductility when compared to the laser peened material.

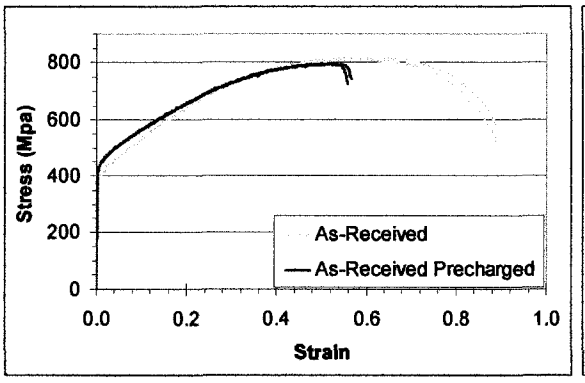

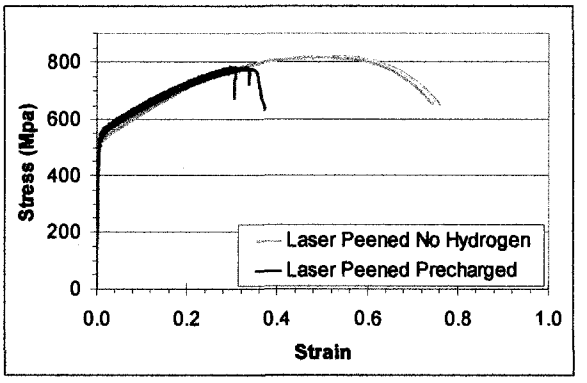

Figure 28 Left – Alloy 22 tensile plots with and without hydrogen precharging.

Figure 29 Right – Alloy 22 tensile plots for the laser peened material with and without hydrogen precharging.

Table 6 Tensile coupon results for the Alloy22 material.

Material	Condition	Environmental Condition	S_y (MPa)	S_u (MPa)	El_u (%)	El_t (%)	RA (%)
Alloy 22	Annealed	non-charged	383	810	58	89	72
		precharged	426	793	52	56	41
	Laser peened	non-charged	473	822	50	78	70
		precharged	508	779	32	34	29

Fractographs of the Alloy 22 material in the as-received and laser peened conditions (Figures 30 and 31) show fracture characteristic of microvoid

coalescence, also called ductile dimple fracture. Large dimples nucleate at the largest inclusions in this steel, while small equiaxed dimples form between these inclusions.

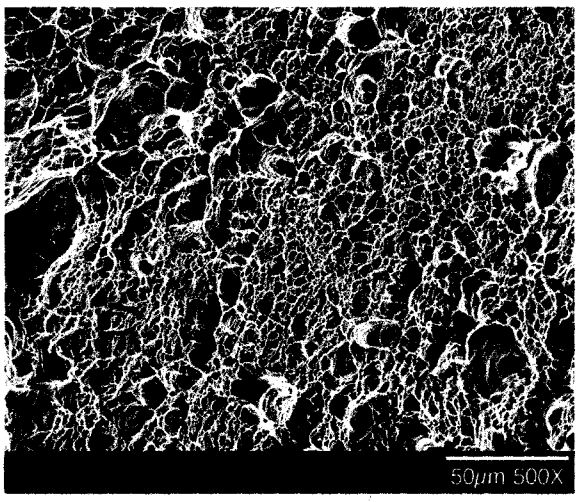

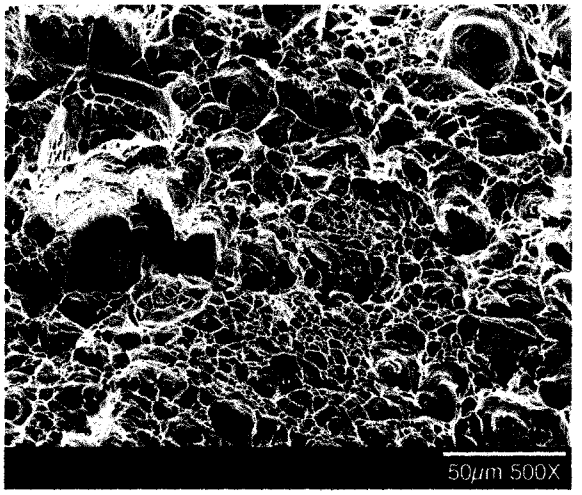

Figure 30 Left – As-received Alloy 22.

Figure 31 Right – Laser peened Alloy 22.

Both images for the hydrogen precharged conditions show mixed-mode fracture: localized areas of dimpled fracture surrounding relatively flat facets. The material displayed some plasticity as evidenced by the ductile dimples; however the overall ductility as measured by elongation and RA were relatively low. The laser peened precharged coupon has larger facets, indicating a further decrease in ductility.

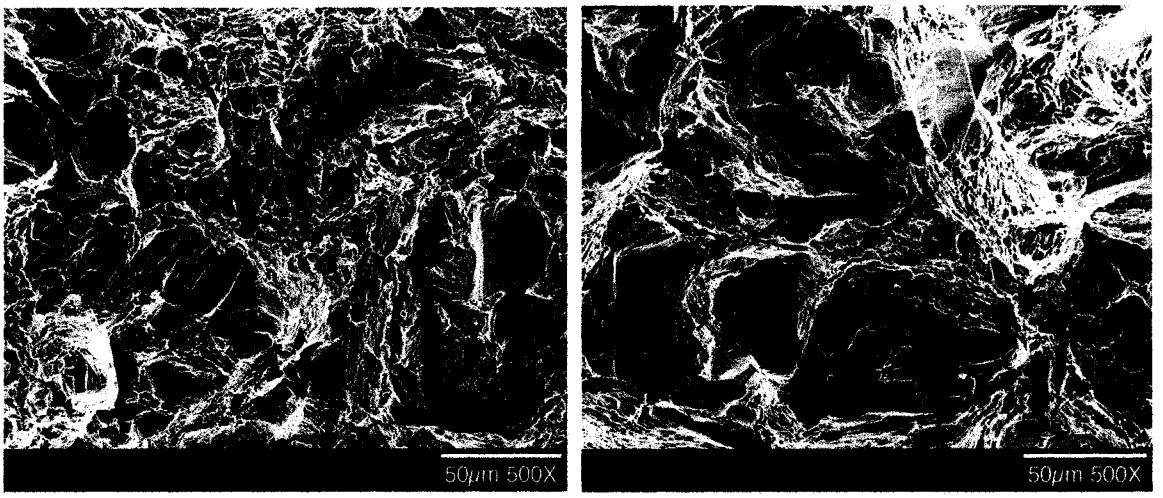

Figure 32 Left – Hydrogen precharged Alloy 22.

Figure 33 Right – Laser peened then precharged Alloy 22.

Tensile Results for 21-6-9

The 21-6-9 material in the as-received condition demonstrated an increase in the ratio of elongation RElu at 1.05. Similarly, the laser peened 21-6-9 also showed an increase in the ratio of elongation of 1.05 due to hydrogen precharding. The as-received material had a smaller RRA due to hydrogen precharging at 0.8 when compared to the laser peened material with an RRA of 0.7.

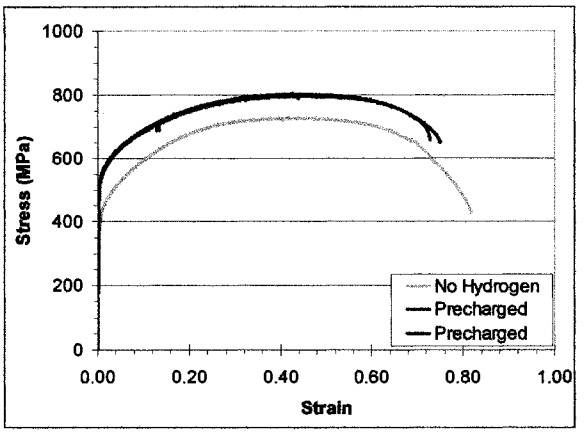

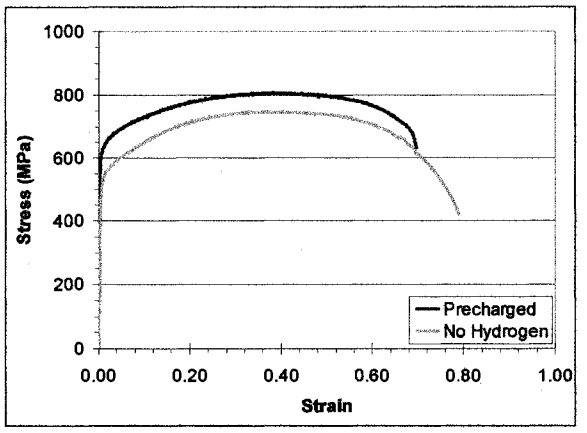

Figure 34 Left - Tensile flow curves for the as-received 21-6-9 coupons with and without hydrogen precharging.

Figure 35 Right - Tensile flow curves for laser peened 21-6-9 with and without hydrogen precharging showing similar trends as the as-received specimens. Hydrogen precharged specimens display a slightly lower elongation to fracture and a somewhat higher strength compared to non-charged specimens.

Table 7 Summary for 21-6-9 tensile properties.

Material	Condition	Environmental Condition	S_y (MPa)	S_u (MPa)	El_u (%)	El_t (%)	RA (%)
21-6-9	Annealed	non-charged	425	735	42	82	74
		precharged	536	800	44	74	59
	Laser peened	non-charged	484	742	38	79	74
		precharged	571	807	40	68	54

Fractographs of the 21-6-9 material in the as-received and laser peened conditions (Figures 36 and 37) show fracture characteristic of microvoid coalescence, also called ductile dimple fracture. Large dimples nucleate at the largest inclusions in this steel, while small equiaxed dimples form between these inclusions.

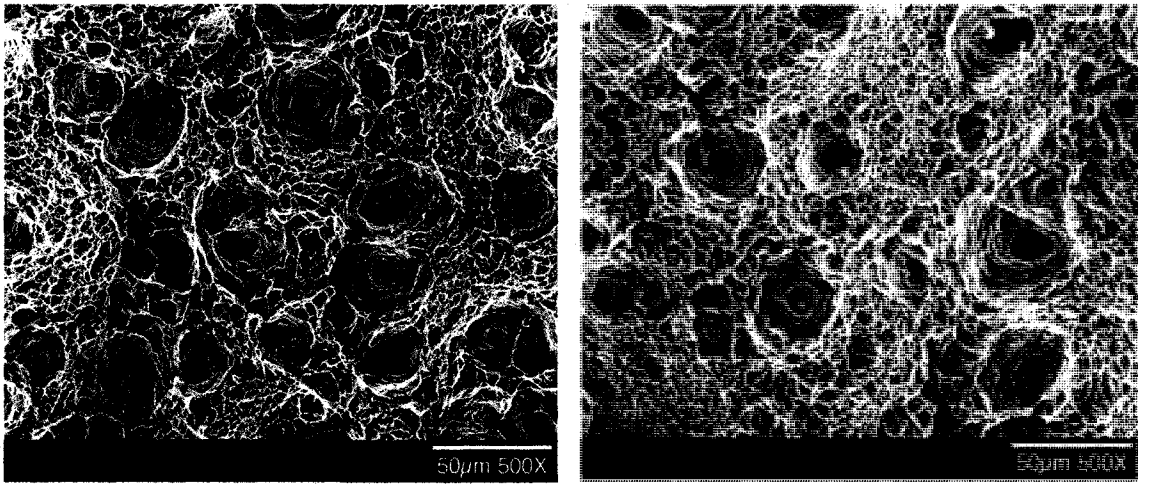

Figure 36 Left - As-received 21-6-9.

Figure 37 Right – Laser peened 21-6-9.

Fractographs of the hydrogen precharged 21-6-9 materials also show evidence of microvoid coalescence (Figures 38 and 39), however, the dimple size was substantially reduced. This indicated that the fracture process was relatively ductile even when the materials were hydrogen precharged. The flat areas on the fracture surface of the laser peened material (Figure 39) were likely artifacts resulting from the fracture surface rubbing against the other half or another surface prior to observation in the SEM.

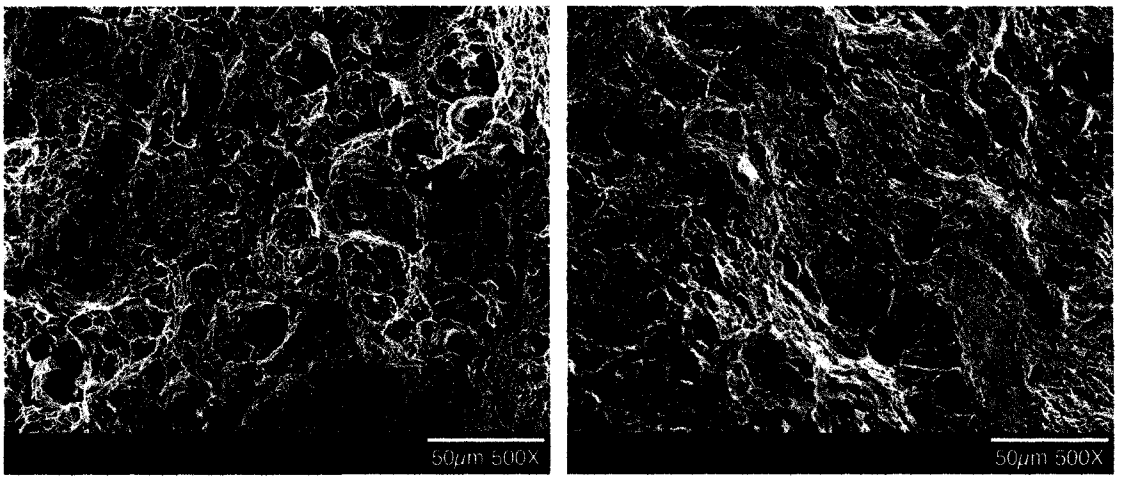

Figure 38 Left - As-received then precharged 21-6-9.

Figure 39 Right – Laser peened then precharged 21-6-9.

Tensile Results for A286

The A286 material showed a slight increase in yield strength and small decrease in ductility due to laser peening. The material exhibited no change in RELu (at 1.0) due to hydrogen precharging compared to 0.93 for the laser peened coupons. The RRA due to hydrogen precharging for the as-received material was measured at 0.45 compared to 0.37 for the laser peened coupons. Hydrogen precharging of the laser peened material produced a larger decrease in Elu and RA compared to the as-received material.

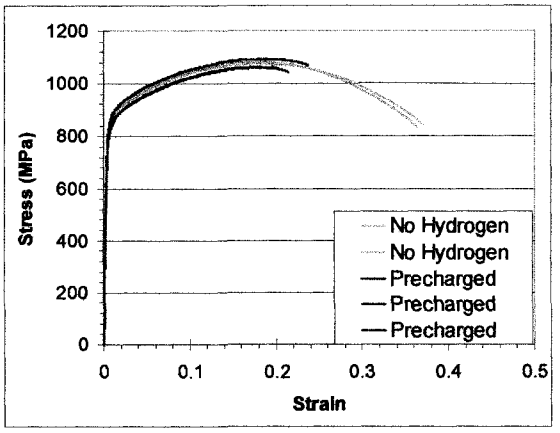

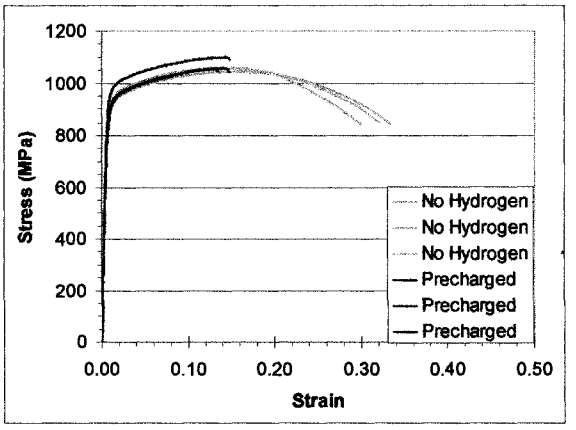

Figure 40 Left - Tensile flow curves for A286 strainless steel with and without hydrogen precharging.

Figure 41 Right - Tensile flow curves for laser peened A286 strainless steel, with and without hydrogen precharging.

Table 8 Summary of tensile results for A286.

Material	Condition	Environmental Condition	S_y (MPa)	S_u (MPa)	El_u (%)	El_t (%)	RA (%)
A-286	Annealed	non-charged	817	1079	18	37	47
		precharged	814	1071	18	22	21
	Laser peened	non-charged	823	1053	15	32	43
		precharged	846	1069	14	14	16

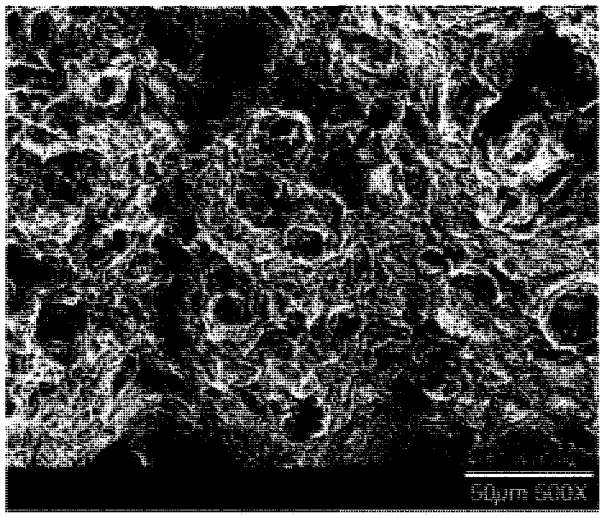

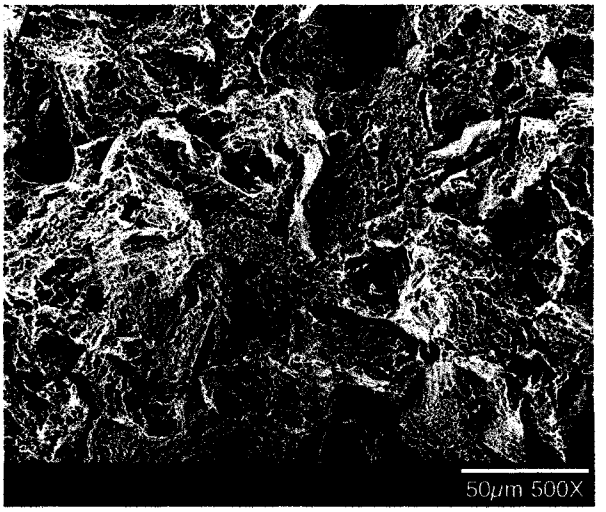

Figure 42 Left - As-received A286.

Figure 43 Right – Laser peened A286.

The fracture surfaces for the as-received precharged A286 and laser peened precharged A286 are in Figures 44 and 45 respectively. Both images show mixed-mode fracture: localized areas of dimpled fracture (A) surrounding relatively flat facets (B). The material displayed some plasticity as evidenced by the ductile dimples; however the overall ductility as measured by elongation and RA were relatively low. The laser peened precharged coupon has a higher frequency of smaller facet surfaces; although the reason for this was unclear.

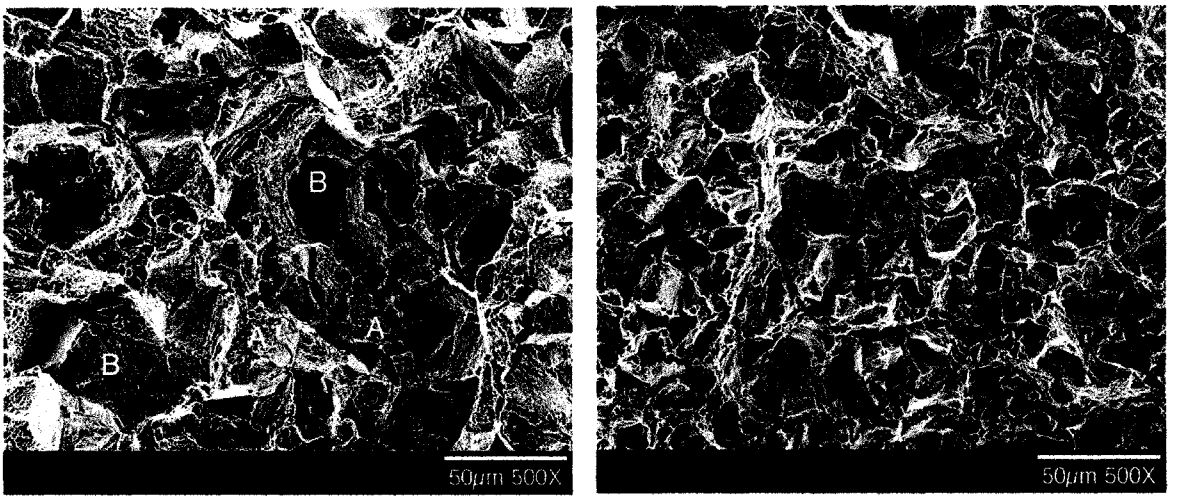

Figure 44 Left - as-received then precharged A286. Fracture areas are denoted with (A) and flat facets are denoted with (B).

Figure 45 Right – Laser peened then precharged A286).

2.5. Fatigue Crack Growth Testing

Fatigue crack growth coupons in A286 (Figure 46) were machined via Electro-Discharge-Machine (EDM) to reduce the residual surface stresses in the material. The recast layer left from the EDM process was removed by lightly polishing.

Fatigue crack growth testing was conducted following the basic procedures of ASTM E647 on a servo-hydraulic test frame (MTS 810). Specimens were precracked under shedding load with a final maximum stress intensity factor (K) of 15 $MPam^{1/2}$. The precrack was grown approximately 1.3 mm (0.05 in) to a length of about 10.7 mm (fractional length, a/W = 0.25). Crack growth was

monitored by the compliance method using MTS Fatigue Crack Growth software. The tests were executed at constant load amplitude at 5 Hz and R = 0.1 (ratio of minimum to maximum load/stress intensity factor). The tests were terminated at crack lengh of approximately 25 mm (a/W = 0.7), which corresponds to a maximum K of about 65 $MPam^{1/2}$. Crack closure was not investigated in this study and all ΔK values represent applied ΔK.

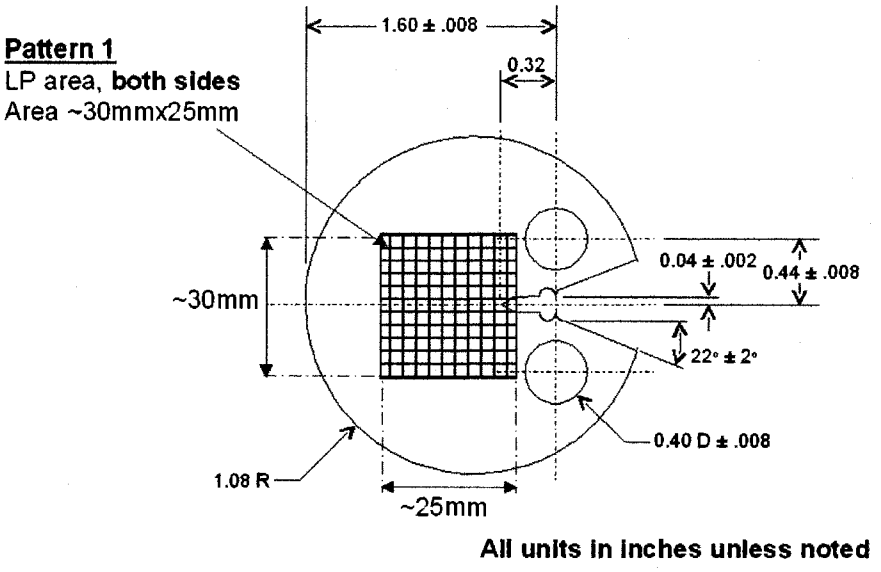

Figure 46 Fatigue coupons for A286.

Table 9 Coupon treatment detail for crack growth test.

Label	Laser-Peening Treatment	Surface Treatment	Environmental Condition	A286 SNs
None	None	As-Recieved	None	AM5
None	None	As-Recieved	Precharged	HE2
6-18-3	6GW/cm2-18ns-3 Layers	Laser peened	None	SN10
6-18-3	6GW/cm2-18ns-3 Layers	Laser peened	Precharged	SN11
8-18-3	8GW/cm2-18ns-3 Layers	Laser peened	None	SN6
8-18-3	8GW/cm2-18ns-3 Layers	Laser peened	Precharged	SN7
10-18-3	10 GW/cm2-18ns-3 Layers	Laser peened	None	SN8
10-18-3	10 GW/cm2-18ns-3 Layers	Laser peened	Precharged	SN9
10-18-2	10 GW/cm2-18ns-2 Layers	Laser peened	None	SN12
10-18-2	10 GW/cm2-18ns-2 Layers	Laser peened	Precharged	SN13

Due to a limited amount of the A286 material, only one coupon was tested at each parameter.

Coupon Testing Results – Crack Growth

Some of the crack measurements came into question during the graphical analysis. A thorough review of the plots in question was outside the scope of this study and have been omitted from Figure 47. The remaining laser peened

specimens plotted in Figure 47 did not show a significant improvement over the varying parameters tested.

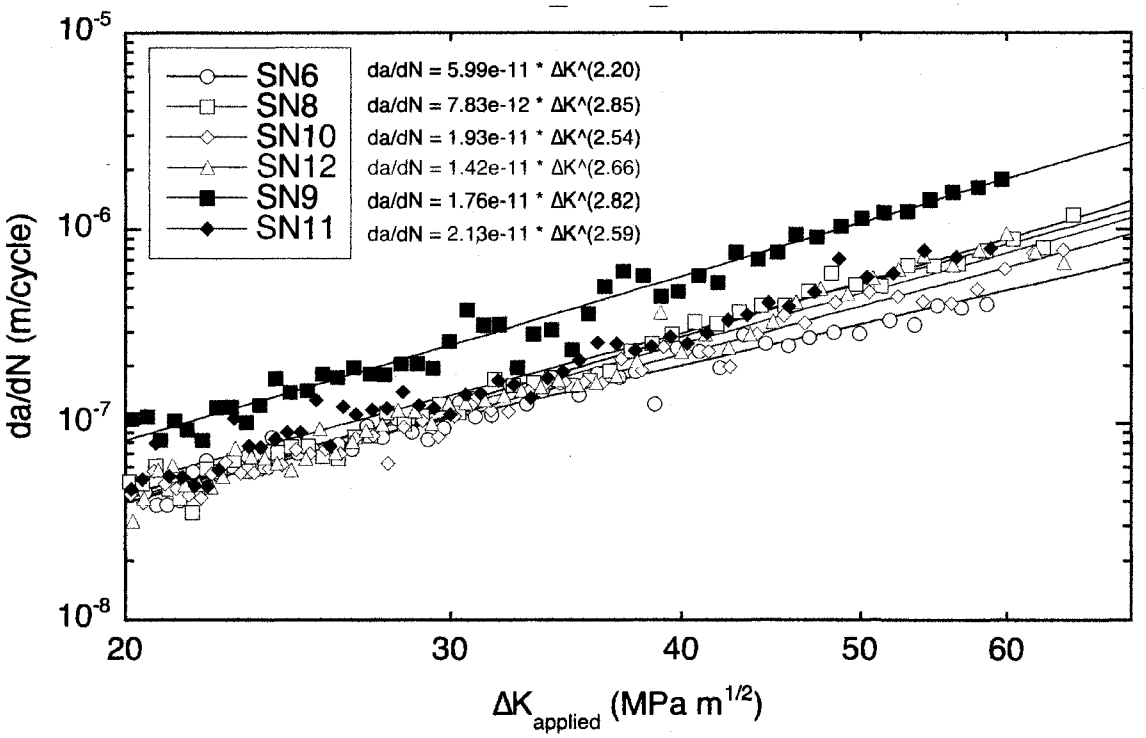

Figure 47 The laser peened coupons do not show significant improvement in crack growth compared to the as-received coupons.

3. DISCUSSION

3.1. Microhardness and SEM Testing in 316L

A previous study by Hill and Liu demonstrated the as-received 316L coupon had a uniform microhardness increase of 30 MHv due to the cathodic charging [42]. In contrast, the laser peened 316L had roughly the same microhardness with and without cathodic charging [42].

The coupons from the previous study by Hill and Liu were imaged in the current study by SEM. These images of the cathodically charged 316L as-received material coupons showed voids throughout the bulk. The laser peened coupon without cathodic charging had both voids and evidence of subsurface cracking. Thus, it seemed that the laser peening treatment induced subsurface cracking in the material. The laser peened 316L cathodically charged coupon had an increase in subsurface cracking compared to the laser peened coupon without cathodic charging. The initial subsurface cracking due to the laser peening process were further expanded due to the introduction of hydrogen by cathodic charging. The minimal increase in hardness of the laser- peened coupon with and without cathodic charging from the study by Hill and Liu could have been due to the increase in subsurface cracking.

3.2. LECO Testing

The LECO hydrogen content testing for the Alloy 22, 21-6-9, and A286 materials showed the same hydrogen content for both the gaseous hydrogen charged base material and the laser peened hydrogen precharged materials. In

each of the three stainless steels tested, the laser peened then precharged samples had the same hydrogen content as the as-received hydrogen precharged materials. Since the laser peening process induces a layer of residual compressive stress at the material surface, it was investigated as a potential surface treatment to act as a barrier to hydrogen transport through steel. However, a reduction in the amount of hydrogen absorbed in the laser peened coupons was not observed. Thus the laser peening does not seem to have delayed the transport of hydrogen into these materials.

3.3. Tensile Coupon Testing

In the three stainless steels tested (Alloy 22, 21-6-9, and A286) the laser peening treatment demonstrated a slight increase in the yield strength of the base material and a small decrease in ductility. After hydrogen precharging, the laser peened stainless steels demonstrated an additional reduction in area which indicated a further decrease in ductility. When compared to as-received precharged material, the laser peened precharged material had a slightly higher yield strength and slightly lower ductility. Since the laser peened stainless steels exhibited further reductions in ductility with hydrogen precharging, the laser peening treatment does not seem to have reduced the hydrogen embrittlement effects in these materials.

3.4. Fatigue Crack Growth

The various laser peening parameters investigated for the A286 stainless

steel did not show significant improvement in fatigue crack growth rates when compared to the as-received material. However the limited number of coupons available in this study prevented the authors from optimizing the laser peening parameters for this material. Further investigation would be needed to quantify the difference in crack growth rates for the laser peened hydrogen charged materials.

4. CONCLUSION

4.1. Effect on Material Properties

The laser peening treatment did not to exhibit much resistance to hydrogen embrittlement effects. Since the treatment did not delay the hydrogen permeation into the surface, the material was further embrittled due to the hydrogen which caused an additional decrease in ductility.

4.2. Effect on Material Performance

The various laser peening parameters investigated did not demonstrate a significant improvement in the crack growth rate for A286. In contrast, laser peening had previously demonstrated a decrease in crack growth rate for Titanium [40]. Previous optimization of laser peening parameters for the particular A286 material tested could not be found in literature. Thus, further investigation would be needed to optimize the laser peening parameters prior to investigating fatigue performance of this particular material in a hydrogen environment.

4.3. Recommendations for Further Study

As stated in the material performance study conclusion, an investigation would first be needed to optimize the laser peening parameters in A286 prior to testing for hydrogen effects.

Further investigation could include the effect of laser peening on fatigue performance in hydrogen environments for previously optimized materials such

as Ti-6-4 [40]. This material has been previously optimized and its performance and residual stress characteristics due to laser peening were well characterized [40].

The mode tested in this study for preventing hydrogen from permeating into the lattice was only for one phase in the material. It would be possible to use laser peening as both a phase converter and compressive stress inducer to reduce the effects of hydrogen permeation into the surface. Studies by Tsay and Liu [50-52] demonstrated that converting the phase of a material could reduce the hydrogen permeation into the bulk. The laser peening treatment could be used as a phase transformer if the ablative layer was not used. This would allow the laser plasma to heat up the material surface, causing it to melt and solidify after the laser pulse. When used in this method a laser "glazing" technique could be applied to the coupon. If this glazing technique was combined with the compressive stress induced by conventional laser peening, further benefit to preventing hydrogen embrittlement could be realized. Although currently beyond the scope of this study to test, it could be an opportunity for further research as there is minimal literature in support of combining the two techniques as a treatment to reduce hydrogen embrittlement.

REFERENCES

1. Hill M, DeWald A, Demma A, Hackel L, Chen H, Dane C, Specht R, Harris F. *Advanced Materials & Processes* 161 i8: 65 2003.
2. Hackle L, Chen H, Dane B, Hill M. "Laser Peening Technology as Developed by LLNL". *LLNL Publication* UCRL-ID-150344, 2002.
3. Saito S, Kikuchi K, Usami K, Ishikawa A, Nishino Y, Kawai M, Dai Y. *Journal of Nuclear Materials* 343: 253-61 2005.
4. Oriani RA. *Acta Metallurgica* 18: 147-157 1970.
5. Symons DM and Thompson AW. *Metallurgical and Meterials Transactions A* 27A: 101-10 1996.
6. Valiente A, Caballero L, Ruiz J, *Nuclear Engineering and Design* 188: 203-216,1999.
7. Fontana GM, Greene ND, *Corrosion Engineering*, 2nd Ed. McGraw Hill 1978. 109-115, 301-303.
8. Steigerwald FW, Schaller FW, and Troiano AR. *Trans. AIME* 218: 832-841 1960.
9. Oriani RA and Josephic PH. *Acta Metallurgica* 22:1065-1074 1974.
10. Beachem CD. *Metall. Trans. A* 3A: 437-51 1972.
11. Eastman J, Matsumoto T, Narita N, Heubaum F, and Birnbaum HK.

Hydrogen Effects in Metals, A.W. Thompson and I.M. Bernstein, eds., TMS, Warrendale, PA 1986, p397-409.

12. Robertson IM and Birnbau HK. *Acta Metall.* 34:353-66 1986.

13. Lee TD, Goldberg T, and Hirth JP. *Metall. Trans. A* 104A: 199-208 1979.

14. Costa E and Thompson AW. *Metall. Trans. A* 13A: 1315-18 1982.

15. Zapfe CA and Sims CE. *Trans. AIME* 11: 225-70 1963.

16. Stephens RI, Fratemi A, Stephens RR, and Fuchs HO. *Metal Fatigue in Engineering* 2nd ed. John Wiley & Sons, Inc. 2001.

17. "Cast Shot and Grit Size Specifications for Peening and Cleaning" , *SAE Handbook*, Vol.1: 8-14, SAE Standard J444, SAE, Warrendale, PA, 1988.

18. Prevey PS, Jayaraman N, Cammett J. "Overview of Low Plasticity Burnishing for Mitigation of Fatigue Damage Mechanisms" Proceedings of ICSP 9 (Paper 260) Paris, Marne la Vallee, France, Sept. 6-9, 2005.

19. Wilde BE, Shimada T. *Scripta Metallurgica* 22: 551-6 1988.

20. Wilde BE and Chattoraj I. *Scripta Metallurgica* 26:627-32 1992.

21. Chattoraj I and Wilde BE. *Scripta Metallurgica* 26: 89-94 1992.

22. Ma CL, Takasugi T, and Hanada S. *Scripta Materialia* 34 No.7: 1131-38 1996.

23. Dane CB, Hackel LA, J. Daly J, Harrisson J. *Materials and Manufacturing Processes* 15, No. 1: 81-96 2000.

24. DeWald AT, Rankin JE, Hill MR, Lee MJ, Chen HL. *Journal of Engineering Materials and Technology* 126: 465 2004.

25. Hackel LA and Chen HL. "Laser Peening—A Processing Tool to Strengthen Metals or Alloys to Improve Fatigue Lifetime and Retard Stress-Induced Corrosion Cracking" *LLNL Laser Science & Technology Report*, UCRL-ID-155327 2003.

26. Chen HL, Rankin JE, Hackel LA, Frederick G, Hickling J, Findlan S. "Laser Peening of Alloy 600 To Improve Intergranular Stress Corrosion Cracking Resistance in Power Plants" *Sixth International EPRI Conference on Welding and Repair Technology for Power Plants*, LLNL UCRL-CONF-203826 2004.

27. El-Dasher BS, Zaleski TM, Gray JJ, Rybak SJ, and Chen HL. *Journal of Applied* Physics 99: 103506 2006.

28. Peyre P, Braham C, Ledion J, Berthe L, Fabbro R, *Journal of Materials Engineering and Performance* 9: 656-662 2000.

29. Smith PR, M. Shepard MJ, Prevéy III, and Clauer AH. *Journal of Materials Engineering and Performance* 9 No.1: 33-37 2000.

30. Preve´y PS and Cammett JT. *International Journal of Fatigue* 26:975-82 2004.

31. Takasugi T, Misawa T, and Saitoh H. *Materials Science and Engineering* A192/193: 413-19 1995.

32. Tal-Gutelmacher E, Eliaz N, Eliezer D, Zander D, Jastrow L, Koester U. Mater. Sci. Eng. A 358: 1–2 219-25 2003.

33. Balasubramaniam R. *Journal of Alloys and Compounds*, 293-295: 279-281 1999.

34. Montross CS, Wei T, Ye L, Clark G, Mai YW, *International Journal of Fatigue* 24: 1021–1036 2002.

35. ASTM Designation: A370-05 "Standard Test Methods and Definitions for Mechanical Testing of Steel Products", *ASTM International* 2005.

36. Brockis JOM, Beck W, Genshaw MA, Subramanyan PK, and Williams FS. *Acta Metallurgica* 19: 1209-18 1971.

37. Kumar P and Balasubramaniam R. *Journal of Alloys and Compounds* 255: 130-134 1997.

38. Porter DA and Easterling KE. *Phase Transformations in Metals and Alloys* 2^{nd} *Ed.,* Chapman & Hall, UK 1992, pp. 73-74.

39. Luong H. "Fatigue life extension and the effects of laser peening on 7050-T7451 aluminum, 7085-T7651 aluminum, and Ti-6Al-4V titanium alloys". *University of California Davis Dissertation*, 2006.

40. Liu KS. "Effects of laser peening on fretting fatigue of Ti-6Al-4V and hydrogen permeation of 316L stainless steel coupons". *University of California Davis Dissertation* 2006.

41. Hackel LA, Chen HL, Dane B, and Hill M, "Laser Peening Technology as

Developed by LLNL", *LLNL Report* UCRL-ID-150344 2002.

42. VanderVoort F. *ASM Handbook* v.8 2000.

43. San marchi C, Balch DK, and Somerday BP. "Effect of High-Pressure Hydrogen Gas on Fracture of Austenitic Steels" *ASME Pressure Vessels and Piping Division Conference,* Proceedings of PVP-2005, PVP2005-71392 2005.

44. San Marchi C and Somerday BP. Technical Reference on Hydrogen Compatibility of Materials (SAND2008-1163). Sandia National Laboratories, Livermore CA 2008.

45. Thompson AW and Brooks JA. *Metallurgical Transactions A* 6A: 1431-42 1975.

46. Aerospace Material Specification "Laser Peening" *SAE International* AMS 2546 2004.

47. San Marchi C, Somerday BP and Robinson SL. *International Journal of Hydrogen Energy* 32: 100-116 2007.

48. Baskes M. DIFFUSE-83. Sandia National Laboratories, Livermore CA (June 1983).

49. Hardwick MF and Robinson SL. Diffuse II: a Hydrogen Isotope Diffusion and Trapping Simulation Program Upgrade. Sandia National Laboratories, Livermore CA 1998.

50. Tsay LW, Lin ZW, Shiue RK, and Chen C. *Materials Science and*

Engineering, A290: 46-54 2000.

51. Tsay LW, Yang TY, and Young MC. *Material Science and Engineering* A311: 64-73 2001.

52. Liu L, Tanaka K, Hirose A, and Kobayashi KF. *Journal of Laser Applications* 15 N.3: 134-44 2003.